

**Studies on Interaction Between Synoptic and Mesoscale  
Weather Elements in the Tropics**

**Report No. 1**

by

Herbert Riehl and Robert P. Pearce

Technical Paper No. 126  
Department of Atmospheric Science  
Colorado State University  
Fort Collins, Colorado

**Colorado  
State  
University**

**Department of  
Atmospheric Science**

Paper No. 126



---

STUDIES ON INTERACTION BETWEEN SYNOPTIC AND MESOSCALE  
WEATHER ELEMENTS IN THE TROPICS

---

Report No. 1

by

Herbert Riehl and Robert P. Pearce

---

Part I: Some Aspects of Cumulus-Scale Downdrafts  
Herbert Riehl, Colorado State University

Part II: Vorticity Budgets Derived from Caribbean Data  
Robert P. Pearce, Imperial College of London

---

Atmospheric Science Paper No. 126

Department of Atmospheric Science  
Colorado State University  
Fort Collins, Colorado

June 1968

## ACKNOWLEDGMENTS

The contribution by H. Riehl was made partly under a research grant by ESSA, No. E 22-138-67(G) to Colorado State University, partly under NSF Senior Postdoctoral Fellowship and sabbatical leave from Colorado State University at Imperial College.

Dr. Pearce wishes to acknowledge the stimulating and constructive comments made during the course of this work by Dr. J.S.A. Green, Imperial College, particularly for pointing out the importance of the twisting terms on the small scale. The computer program development was carried out by Mr. R.A. Drayton, and the results in Figs. 8-12, Part II, plotted by Miss A. Jowett.

Both authors wish to express their sincere thanks to Professor P.A. Sheppard, Head of the Meteorology Department, Imperial College, who made all facilities in the department and electronic computer time available on a most liberal scale. Miss M. Street performed a large part of the plotting and computing work; she also drafted the illustrations. Her excellent efforts are very much appreciated.

Part I  
SOME ASPECTS OF CUMULUS-SCALE DOWNDRAFTS

H. Riehl

Introduction

In spite of extensive release of latent heat of condensation in synoptic-scale disturbances of the tropics, the air situated in the areas with greatest synoptic-scale convergence and precipitation is often relatively dense with respect to the outside of these disturbances (Riehl 1948). The relatively dense air may extend from the sub-cloud layer to the middle troposphere and occasionally even to the high troposphere. In contrast, disturbances with a central core less dense than their surroundings also occur (Riehl 1959). These need not be of hurricane intensity; steady state may be achieved with weak wind fields (Elsberry 1965).

The cold core structure of disturbances can be explained thermodynamically by postulating net mass ascent of the atmosphere in a convergence zone, plus ascent of cumulus towers and outward mixing of relatively light air from these clouds (Riehl 1948, 1954). Such ascent, with meso-scale structure, may actually lead to net warming of the cloudy region in the upper troposphere with respect to its environment. A neutral point of the flow around 200 mb, or even anti-cyclonic circulation, is then found above the layer with high cyclonic vorticity where cumulonimbus anvils widely reach the 200-mb level. In such a setting release of latent heat of condensation can contribute toward maintaining the kinetic energy of disturbances and of the primary circulation (Riehl 1959, 1963).

Research aircraft flights conducted in a wave in the easterlies,

intercepted in the western Caribbean during August 1964, have pointed to another complicating mechanism in the lower troposphere (Riehl 1967). It was observed that moisture and temperature, and hence also the equivalent potential temperature ( $\theta_e$ ), decreased below 800 mb from the clear surroundings toward the air with heaviest cloudiness. Barring any airmass change of frontal nature, which was not involved, this phenomenon could only be explained by calling on downdrafts from higher levels, where  $\theta_e$  is normally much lower than near the surface in the tropical atmosphere. The only mechanism capable of producing active downdrafts is evaporation from falling rain. Downdrafts initiated by evaporation have effects on the thermal and moisture structure of a tropical disturbance resembling those introduced by a middle latitude front. Only, in this case, the "cold air" comes from higher altitudes rather than from higher latitudes. This suggested sequence of events is novel at least in that it accepts the possibility of modification of large-scale disturbances by smaller-scale events within their envelope, and that the meso-scale overturning can be an important deterrent of hurricane formation through introduction of air with relatively low heat content into the surface layer.

Cooling of the air near the surface has often been noted in rain areas of the tropics. However, the suggestion has at least been implicit that this cooling occurs at constant  $\theta_e$ , that is the temperature falls as the moisture in the air rises and both drybulb and dewpoint approach the wetbulb temperature. The observations in 1964 thus point to a completely different process. Meso-scale downdrafts carrying air with low  $\theta_e$  to the surface have been known for a long time as thunderstorm downdrafts. It is now suggested that the atmosphere may be transformed on the synoptic scale by prolonged downdraft activity. As a result, the vertical gradient of  $\theta_e$  weakens even though, over the tropical ocean, the heat flux from below always acts to restore the gradient. In the extreme case  $\theta_e$  would become uniform with height, a transformation already studied by Rossby (1932) for dry air.

The purpose of this paper is to present initial results from several Caribbean disturbances which have been analysed with a view to determining whether the downdraft effect could be observed regularly and whether it was to be found in both steady state and in hurricane producing waves in the easterlies. Next, the energy transfer from the ocean surface is analysed in relation to changes in the moisture structure of the subcloud layer. Finally, an attempt is made to compute turbulent mass and vorticity transfer along the vertical within the synoptic-scale setting preliminary to considering other forms of turbulent exchange.

#### Vertical Distribution of Moisture and Equivalent Potential Temperature

Fig. 1 shows the location of the rawinsonde stations in the Caribbean area. Not all stations were in operation during each of the periods analysed; the best coverage was in the late 1950's, deteriorating later.

Five cases were selected yielding fourteen map periods for analysis. Of these, two developed into hurricanes and three did not. The cases were chosen so as to provide the greatest possible variation of wave structure:

14-16 September, 1958; a strong stable wave travelling westward at 17 knots; anticyclonic flow in the high troposphere.

19-22 September, 1959; large amplitude wave travelling westward at 17 knots, then decelerating. After several abortive attempts a circulation formed near the east end of Cuba and eventually became a hurricane.

6-8 August, 1964; the wave discussed in the Introduction, which did not develop into a hurricane, is here analysed just prior to the period with aircraft missions.

12-14 September, 1963; a warm core wave moving westward in a

steady state at 15 knots. The circulation was strong at the surface, but it was completely damped out as low as 700 mb -- a remarkable occurrence (Elsberry 1965).

2-5 October, 1958; rapid development at first of a low-level wave, and then of a hurricane, from initial high-tropospheric trough. Rate of motion was 17 knots at first, then slowed to 5 knots or less.

A few illustrations from the large amount of analysed material follow. Vertical time sections of the moisture during wave passage at particular stations are well suited to demonstrate the effect of any downdrafts present. In order to obtain a synoptic-scale view of the moisture variations, the specific humidity at many stations was first plotted against time at 1000, 850, 700, 500, 400, and 300 mb and a smooth profile drawn at each level maintaining vertical continuity. From the smoothed values the specific humidity of a mean tropical atmosphere for the hurricane season (Jordan 1958) was next subtracted. This eliminates most of the vertical gradient and makes it possible to bring out the horizontal and vertical changes in specific humidity.

Fig. 2a shows a specific humidity anomaly time section as just described for the September 1958 wave; this time section reveals moisture changes similar to those observed by aircraft in August 1964, already discussed. Ahead (west) of the wave axis moisture is high at low levels, with dryness in the higher troposphere. On the rear (east) side the reverse holds. Whereas one might have expected a thick layer with positive moisture departure from the mean from the ground upward, actually specific humidity is lower than in the outskirts of the wave in the lowest 200 mb. In view of the rapid displacement of the wave, the motion of the air relative to the system is mainly from the west, that is air crosses from the west side to the east side of the axis. Convergence begins before the air reaches the axis, reflected at first by a rise in specific humidity throughout the troposphere. Then, in

the heavy convergence zone east of the axis (Fig. 3) the increase in moisture continues at 700 mb and higher, while drying occurs at the lower levels. A similar sequence of events holds for air approaching the convergence zone from south or south-southeast on relative trajectories with long duration of convergence.

Almost the same moisture pattern is present at Kingston one day later (Fig. 2c). The  $\theta_e$  profiles at both stations (Figs. 4a-b) show the marked reduction of vertical gradient across the wave, a low-level decrease of  $\theta_e$  taken as evidence for the downdraft mechanism, and an overall increase of  $\theta_e$  for the troposphere which follows from the net tropospheric convergence.

Comparison with the hurricane forming cases shows, surprisingly, that the same pattern prevailed in the specific humidity time sections prior to development and even during development except in a small area around the forming center. Thus, at Guantanamo in October 1958 (Fig. 5a), we see virtually a replica of the September 1958 sections at a late stage when hurricane formation was well under way close to Gran Cayman. However, at Kingston, close to the forming center, a dry layer east of the axis is no longer evident (Fig. 5b), and this is also true at Gran Cayman (Fig. 5c), a station actually crossed by the forming center. Correspondingly, the  $\theta_e$  profiles trend toward a diminished vertical gradient in the convergence area, with large increases in  $\theta_e$  at both Kingston and Gran Cayman (Figs. 6a-c).

An attempt to prepare a moisture time section for the unusual wave of September 1963 failed because of excessive scatter in the reported specific humidities. However, the whole middle and upper troposphere remained very dry, with specific humidities well below those of the mean tropical atmosphere. In fact, except in the layer from the surface to 850 mb, the specific humidity attained a minimum at several stations as the axis passed. This suggests very little convective activity and upward moisture transport there. Satellite pictures, as

well as personal observations at Puerto Rico, confirm this conclusion. Ahead of the wave skies were very clear; to its rear, heavy cloudiness and precipitation expected because of the large amplitude of the wave at the surface did not materialise to the extent anticipated. Correspondingly, the  $\omega$ -field at 850 mb ( $\omega = dp/dt$ ) was very weak, with only 1-2 mb/hr ascent compared with 4-5 mb/hr over a larger area for the cases with heavy convection. A diagram of  $\theta_e$  composited by Elsberry (1965) over the three days when the wave could be followed, showed slightly enhanced  $\theta_e$  near the axis at all levels below 500 mb, in accord with the observed scarcity of showers and the corresponding absence of downdrafts from evaporation of falling rain.

It has been demonstrated, using moisture cross sections and vertical  $\theta_e$  profiles, that a redistribution of heat and moisture frequently occurs in synoptic-scale convergence zones of the tropics, so that the vertical gradient of  $\theta_e$  is reduced compared to the surroundings and the  $\theta_e$  is actually reduced in the low troposphere below approximately 800 mb. Further, such lowering of  $\theta_e$  can only come about, in the situations under discussion, through importation of air with low  $\theta_e$  from the middle troposphere; the only process known to make such importation mechanically possible in a short time (hours) is downward buoyancy produced by evaporation of rain drops falling into unsaturated air. Thus it is suggested that the downdraft mechanism, well known in thunderstorms on the meso-scale, can partly shape the structure of synoptic disturbances when operating on the air in a convergence zone for 12-24 hours. Since wave speed and low-level trade wind speed are almost equal, the condition that the low-level air must remain in the convergent zone for a relatively long time is well met. In fact, there were always rather large areas with relative motion of only 1 knot, hence areas with virtually zero relative motion. An exception may occur when the shower activity is very weak; then an increase in  $\theta_e$  may occur at low levels without being hindered by downdrafts carrying air with low  $\theta_e$  to the surface.

From the change in the  $\theta_e$  profiles across the waves, it follows also that the latter act as a very effective mechanism for upward heat transport. As we have seen, much of the air passing through the waves appears to come from the west. Thus one may think of the waves as marching perturbations which continuously overtake air with energy concentration in the layer of the trade wind clouds and with a relatively steep lapse rate. Through the convergence associated with the waves the energy is transported upward and the lapse rate is reduced, with lower cooling and upper warming, and a transition from cumuliform to stratiform cloud types. Thus, the energy gained by the air from the sea and stored in the trade wind layer, is removed by means of the waves to the middle and high troposphere.

#### Specific Humidity of the Surface Layer

Over the tropical oceans latent and, to a much smaller degree, sensible heat is transferred continuously from the surface to the atmosphere. It has often been suggested that this heat flow gradually may increase surface drybulb and dewpoint temperatures, so that ascending air will follow a moist-adiabatic path sufficiently warm to initiate tropical storm formation from release of latent heat energy. Climatically, of course, it is known that the mean sea level trajectories cross toward higher sensible and latent heat as they approach the equator and that cumulus ascent paths occur at increasingly warm temperatures. However, the increase of heat content of the surface layer does not depend on the energy transfer from the ocean but on the divergence of energy flux. Hence the relation between air-ocean energy exchange and variations in the energy of the surface air should be reexamined in the light of the existence of the buoyant downdrafts. Such an examination should also give some indication regarding the importance of so-called oceanic "hot spots," areas with positive temperature anomaly of a few tenths degree C with respect to their surroundings.

Evaporation: The latent heat flux from the sea can be computed with the turbulence formula (Jacobs 1942)

$$Q_e = c_D \rho L (q_{\text{ocean}} - q_{\text{air}}) V_{\text{air}}, \quad (1)$$

where  $c_D$  is the drag coefficient,  $\rho$  the air density,  $L$  the latent heat of evaporation,  $q_{\text{ocean}}$  the saturated specific humidity at the temperature of the ocean surface, and  $q_{\text{air}}$  and  $V_{\text{air}}$  the specific humidity and wind speed at ship's deck level (about 10 m). This formula and its shortcomings have been discussed widely in the literature. For constants we shall use  $c_D = 1.5 \times 10^{-3}$ ,  $\rho = 1.15 \times 10^{-3} \text{ g cm}^{-3}$ ,  $L = 600 \text{ cal/g}$ . The variables are  $V_{\text{air}}$  and  $q_{\text{ocean}} - q_{\text{air}}$ . Of these,  $V_{\text{air}}$  can be determined with reasonable accuracy from ship observations together with wind measurements at 1,000 - 2,000 feet over land, since the change of wind speed with height above ship's deck level is normally small in the trades. The ship winds were usually too few at any one map time to establish an isotach pattern. Hence the maps six hours before and after were also used and  $V_{\text{air}}$  plotted on a composite chart in wave coordinates.

The quantity  $q_{\text{ocean}} - q_{\text{air}}$  presented much greater difficulties, since neither variable is well reported. A uniform ocean temperature of  $83^\circ\text{F}$  ( $q_{\text{ocean}} = 25 \text{ g/kg}$ ) from climatological data was assumed for the central and western Caribbean; this temperature may be somewhat in error. However, the most unreliable calculation is that of  $q_{\text{air}}$ , although it should be the easiest measurement, as it depends only on a good wetbulb reading. Actually dewpoint (and wetbulb) temperatures -- over the ocean, small or flat islands, and other coast lines -- rarely fell into a readily analysable pattern. Even after compositing three six-hour surface maps with consideration of diurnal variations, it still proved necessary first to determine the average dewpoint in 200-mile squares and then to fit an analysis to these values. Fig. 7 shows the result of this analysis procedure for one situation when data

was unusually plentiful and consistent in the most critical areas. A center of relatively dry air followed the wave axis, and a pattern of roughly this form was found on nearly all maps. An incipient hurricane was present (heavy dot) at the time shown in Fig. 7; yet observations of low dewpoint near this center were common. Reports of 23°C dewpoint and  $\theta_e$  in the 345°-350°K range were frequent, suggesting a cloud base much below that of normal trade wind cumuli and surface properties indicative of downdrafts.

In spite of the limitations mentioned, the evaporation charts could all readily be drawn. The pattern was rather uniform, though strongest evaporation varied from 1 to 2 cm/day. Because of the similarity in pattern, only one composite chart for all cases has been reproduced (Fig. 8). The wind speed  $V_{air}$  is the quantity which mainly determines the characteristics of the pattern; in each instance a horseshoe-shaped area of strongest wind (near 30 knots) was present in the northern part of the waves. This was also the area where the air moved from the east relative to the waves. Highest surface wind speeds, and largest evaporation, occurred on 15 September 1958, on the occasion of a non-developing wave.

The specific humidity difference between sea and air also affects the pattern, though only to a lesser extent. The error margin is at least 10-15 per cent. The sensible heat flow from the sea is also estimated at 10-15 per cent of the latent heat flux in disturbances short of tropical storm intensity. Even though the sensible heat transfer is enhanced proportionately more than the latent heat transfer in disturbances (Garstang 1967) the sensible heat flow was not computed because it is no larger than the error margin in the latent heat flow computation. The evaporation, after multiplication with the proper constant, will be taken to represent the total energy transfer from the sea.

Surface trajectories: We now turn to the relation between energy transfer from sea to air and changes in energy along the surface trajectories of the synoptic-scale motion. Assuming steady state with respect to the moving waves in the first approximation,

$$dQ/dt = V_r \partial Q / \partial s_r, \quad (2)$$

where  $V_r$  is the wind speed relative to a coordinate system moving with the wave,  $s_r$  is distance along the relative streamline and  $t$  is the time. Quite generally,  $Q = gz + c_p T + Lq + K$ , where  $g$  is acceleration of gravity,  $c_p$  specific heat at constant pressure,  $T$  temperature, and  $K$  the kinetic energy per unit mass. For present purposes  $K$  may be neglected as a very small term in a general heat balance equation, and the potential energy  $gz$  remains zero along surface trajectories. Neglecting variations in  $c_p T$  for the reasons that led to omitting the sensible heat transfer from the sea,

$$dQ/dt = L V_r \partial q / \partial s_r, \quad (3)$$

in which form the equation is readily evaluated from moisture and relative motion charts as indicated in Fig. 7.

Figs. 9-13 present the results, averaged for each of the five cases, and with the relative motion vectors of the surface flow added. If the calculations are valid for the whole of the subcloud layer, as is presumably true, then the units can be changed to cal/day/unit area below the subcloud layer through multiplication by  $6 \times 10^6$ , approximately, indicating that the values range up to 25 per cent of the energy transfer from the ocean.

The outstanding feature revealed by Figs. 9-13 is that there was no correlation with the evaporation which, as stated earlier, always had the same shape as in the composite chart of Fig. 8. Of outstanding interest are the centers with negative  $d/dt$ , located close to the

areas with strongest evaporation. Scatter diagrams (not reproduced) also confirm that the magnitude of the evaporation does not determine the magnitude, or even the sign, of  $L dq/dt$  in the subcloud layer. One cannot hope to find, as indeed one should not, a simple relation between energy transfer from the sea and energy changes in the surface layer.

It becomes necessary to consider turbulent transports. We shall here restrict consideration to vertical exchanges. If, at the top of a volume moving along the synoptic relative trajectory, the upward heat transfer is greater than the importation from the ocean, the volume will undoubtedly lose heat. Several years ago A. Pike<sup>1</sup> demonstrated that along surface trajectories of the mean motion in the Atlantic trades drying out could take place under strong anticyclonic conditions. Presumably very dry air was mixed down from a strong trade wind inversion toward the surface. The concept of dewpoints decreasing slowly for several days along the surface air flow in the tropics, or even remaining constant, in the presence of continuing evaporation from the sea may be considered unusual, but its validity is demonstrable. In this study we have found a second mechanism capable of lowering the dewpoint of the surface air, this time in convergence zones: the downdraft from precipitation cooling which intrudes into the surface layer. It follows that the heat content of air ascending in cumulus towers depends heavily on the downdraft rate, and on the properties of the air reaching the surface in downdrafts. The energy flow from the sea will tend to be large, where the specific humidity of the surface air is least, hence also  $q_{\text{ocean}} - q_{\text{air}}$  largest. We conclude that the rate of heat transfer from the ocean, and small spatial variations associated with local gradients of ocean temperature, are unlikely to have

---

<sup>1</sup>Department of Atmospheric Science, Colorado State University, Fort Collins, Colorado, mimeographed, 1961.

an important bearing on intensification of waves in the easterlies. The essential factor would appear to be the suppression of importation of air with low energy content from the middle troposphere toward the surface. This is primarily accomplished if  $\partial\theta_e/\partial z$  becomes small or zero. In that connection it is of interest that all five cases show an area with positive  $L dq/dt$  downstream along the relative trajectories from the negative areas. While data are insufficient for a complete description, the arrangement of the patterns suggests that air entering the convergence zones at first is strongly subject to lowering of the surface heat content by downdrafts since  $\partial\theta_e/\partial z$  there is large. Through the overturning plus convergence, however, the vertical redistribution of heat described at the beginning of this report takes place. Therewith  $\partial\theta_e/\partial z$  becomes small and ineffective in opposing the occurrence of positive  $L dq/dt$  in the surface layer from heat transfer from the ocean.

It is seen that the evaporation from falling rain is a powerful deterrent of amplification of waves in the easterlies, from the thermodynamic standpoint. A quantitative model of downdraft mechanism is being developed in order to permit inclusion of this effect in calculations when synoptic-scale observations are available and events on the meso-scale must be treated on a parametric basis. Another matter becomes of vital interest for a quantitative description of tropical disturbances: the synoptic-scale vertical motion. Its determination and its relation to the vorticity field is considered in Part II which follows.

## References

- Elsberry, R., 1965: On the mechanics and thermodynamics of a low-level wave in the easterlies. Dept. Atmos.Sci., Colo. State Univ., Fort Collins, Colo. 31 pp, mimeographed.
- Garstang, M., 1967: Sensible and latent heat exchange in low latitude synoptic scale systems. *Tellus*, 19, pp. 492-509.
- Jacobs, W.C., 1942: On the energy exchange between sea and atmosphere. *J. Marine Res.*, 5, pp. 37-66.
- Jordan, C.L., 1958: Mean soundings for the West Indies area. *J. Meteor.*, 15, pp. 91-97.
- Riehl, H., 1948: On the formation of West Atlantic hurricanes. Dept. Meteor., Univ. Chicago, Misc. Rept. 24, Part 1.
- Riehl, H., 1954: *Tropical Meteorology*. McGraw-Hill Book Co. Inc., New York, 394 pp.
- Riehl, H., 1959: On the production of kinetic energy from condensation heating. *The Atmosphere and the Sea in Motion*. B.Bolin, Ed., Rockefeller Institute Press, New York, pp. 381-399.
- Riehl, H., 1963: Stationary aspects of the tropical general circulation. *Geofisica Internacional*, Mexico, 3, pp. 53-68.
- Riehl, H., 1967: Varying structure of waves in the easterlies. *Proc. International Symposium on Dynamics of Large-Scale Processes in the Atmosphere*, Moscow, pp. 411-416.
- Rossby, C.-G., 1932: Thermodynamics applied to air mass analysis. *Mass. Inst. Tech. Meteor. Papers* 1, No. 3.

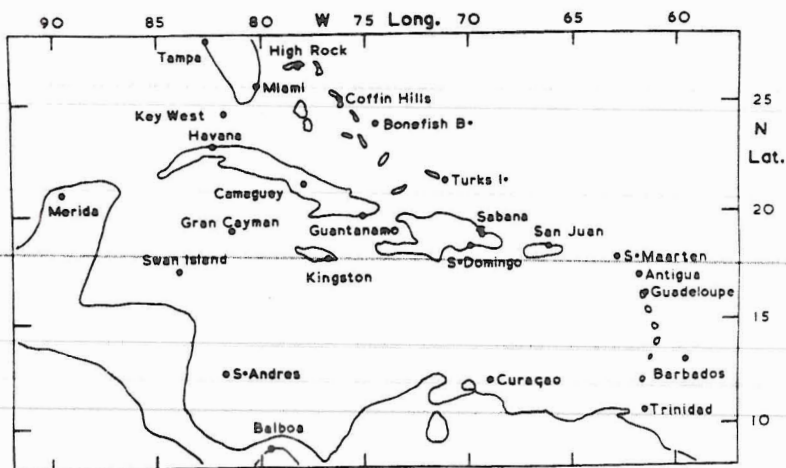


Fig. 1. Rawinsonde stations in the Caribbean area.

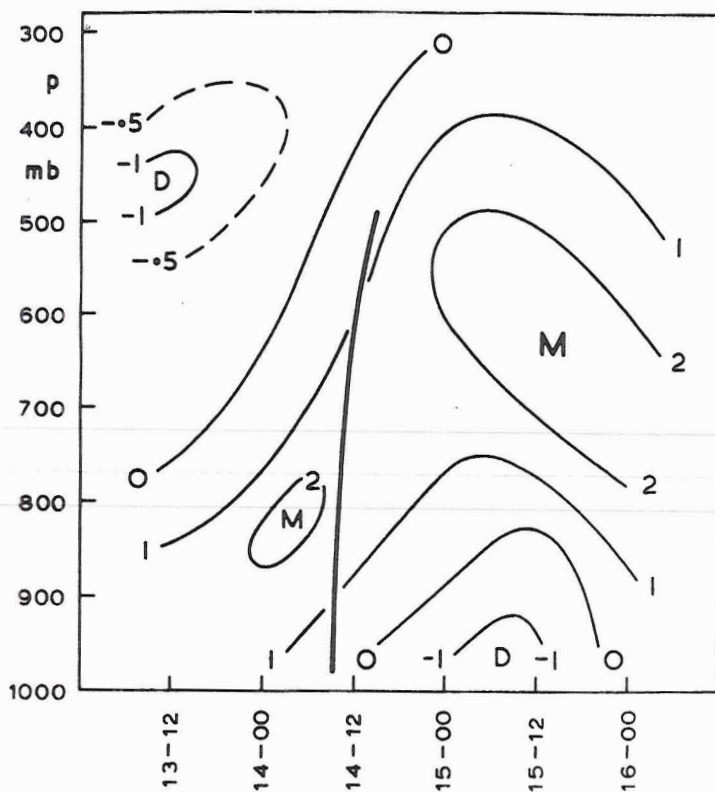


Fig. 2a. Pressure-time cross section of deviation of specific humidity (g/kg) from the average summer Caribbean atmosphere, for Sabana de la Mar, Dominican Republic, 13-16 September 1958. Dates and times (GMT) are given on the abscissa. Heavy solid line is wave axis.

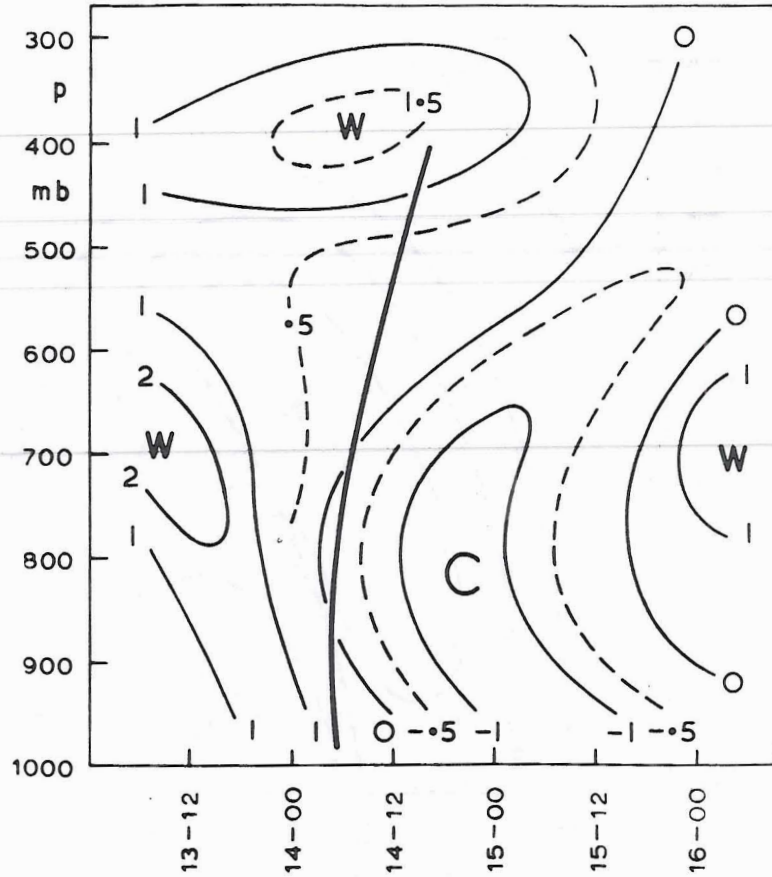


Fig. 2b. Pressure-time cross section of deviation of temperature ( $^{\circ}\text{C}$ ) from the average Caribbean summer atmosphere, for Sabana de la Mar, 13-16 September 1958.

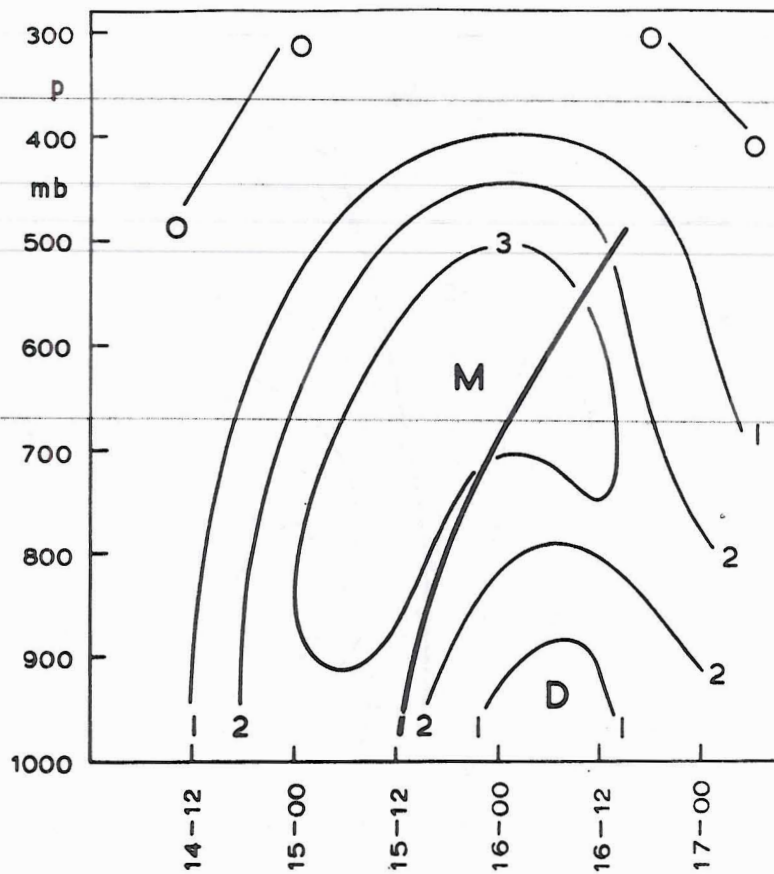


Fig. 2c. Pressure-time cross section of deviation of specific humidity (g/kg) from the average summer Caribbean atmosphere, 14-17 September 1958, for Kingston.

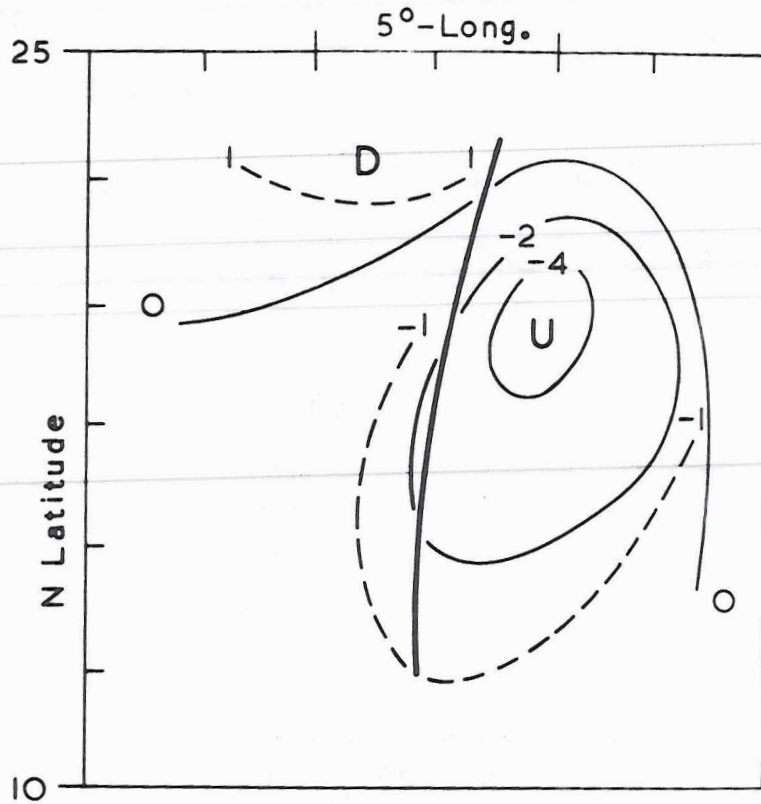


Fig. 3. 850-mb chart showing  $\omega$  (mb/hr) for 15 September 1958. Heavy line is wave axis. Area of map extends from 10° to 25°N and over 15° longitude centered on the wave axis in the west-central Caribbean.

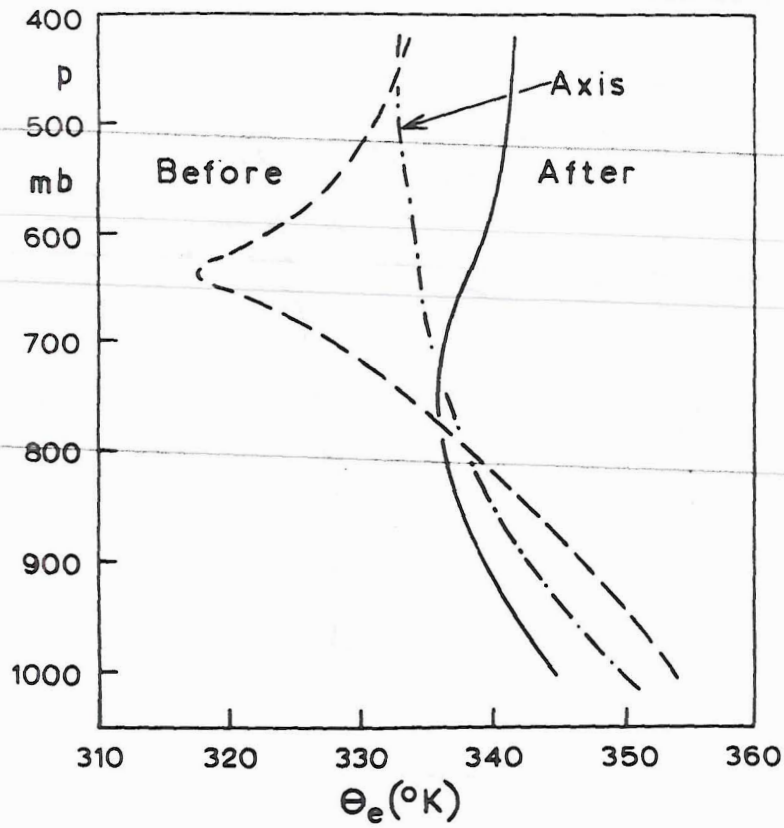


Fig. 4a. Profiles of equivalent potential temperature against pressure at Sabana de la Mar 12 hours before, at the time of, and 12 hours after passage of the wave shown in Figs. 2a-b at the surface.

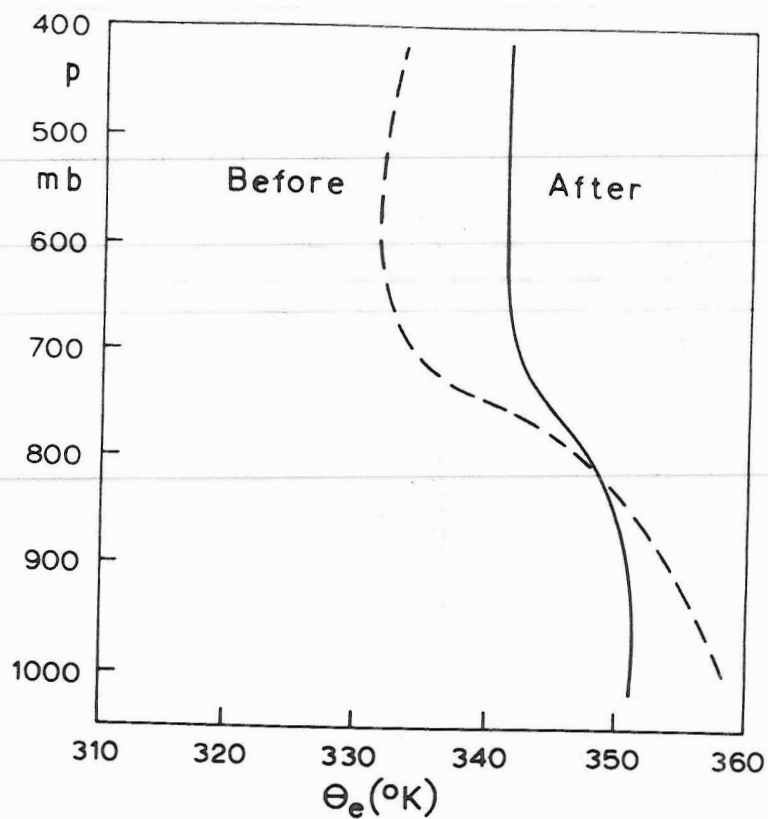


Fig. 4b. Profiles of equivalent potential temperature at Kingston before and after passage of wave shown in Fig. 2c.

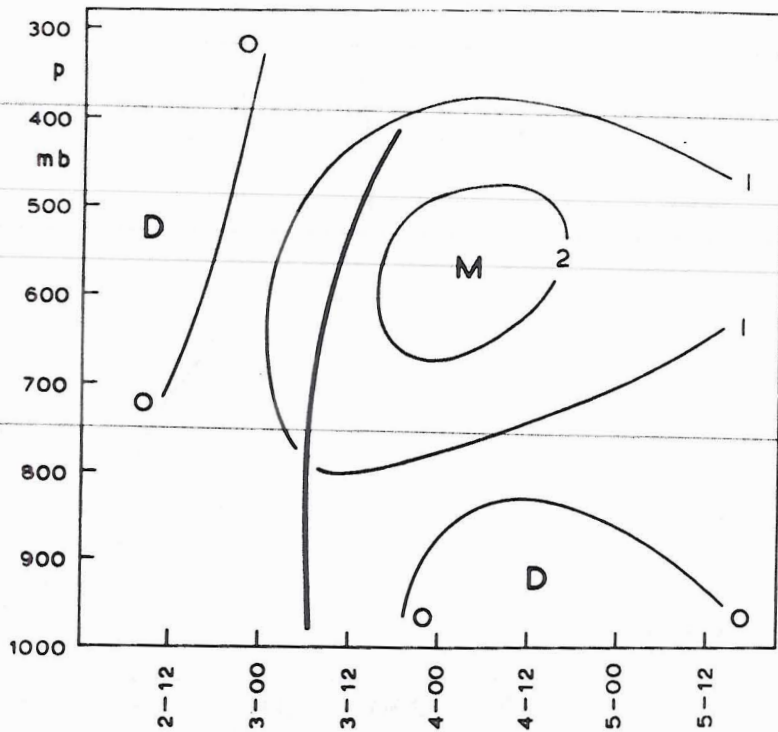


Fig. 5a. Pressure-time cross section of deviation of specific humidity (g/kg) from the average summer Caribbean atmosphere, 2-5 October 1958, for Guantanamo Bay.

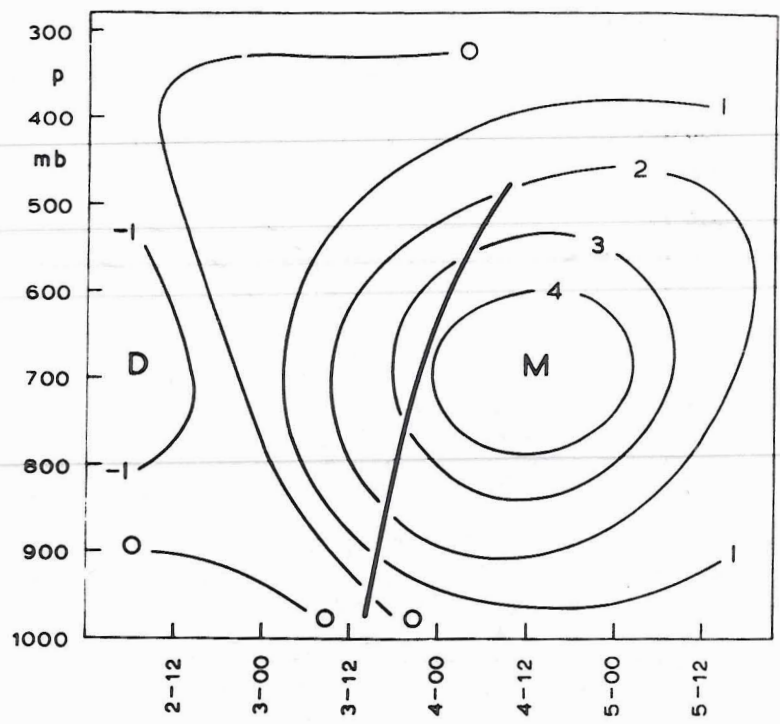


Fig. 5b. Pressure-time cross section of deviation of the specific humidity (g/kg) from the average summer Caribbean atmosphere, 2-5 October 1958, for Kingston.

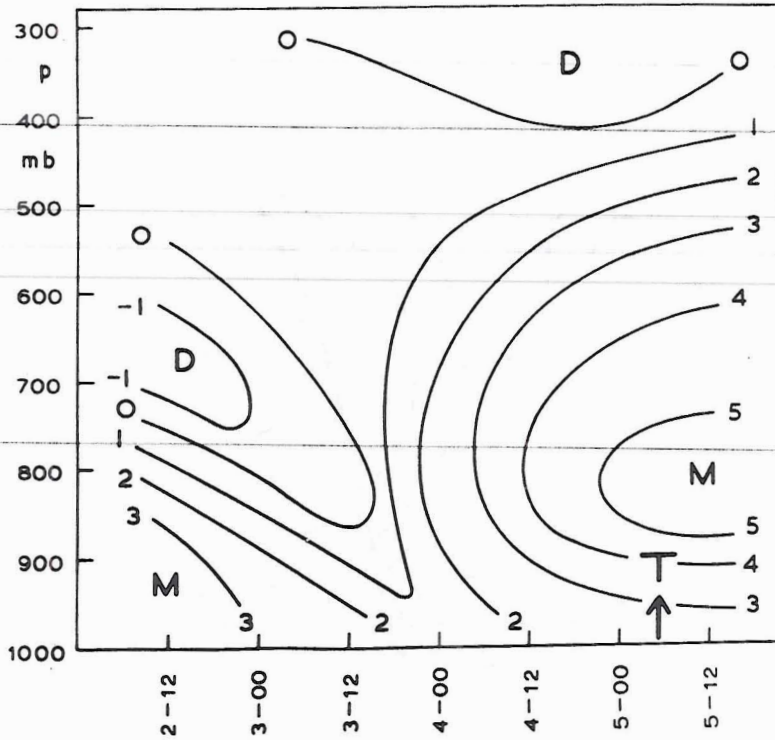


Fig. 5c. Pressure-time cross section of deviation of the specific humidity (g/kg) from the average summer Caribbean atmosphere, 2-5 October 1958, for Gran Cayman. Heavy arrow indicates time of passage of tropical storm center across station.

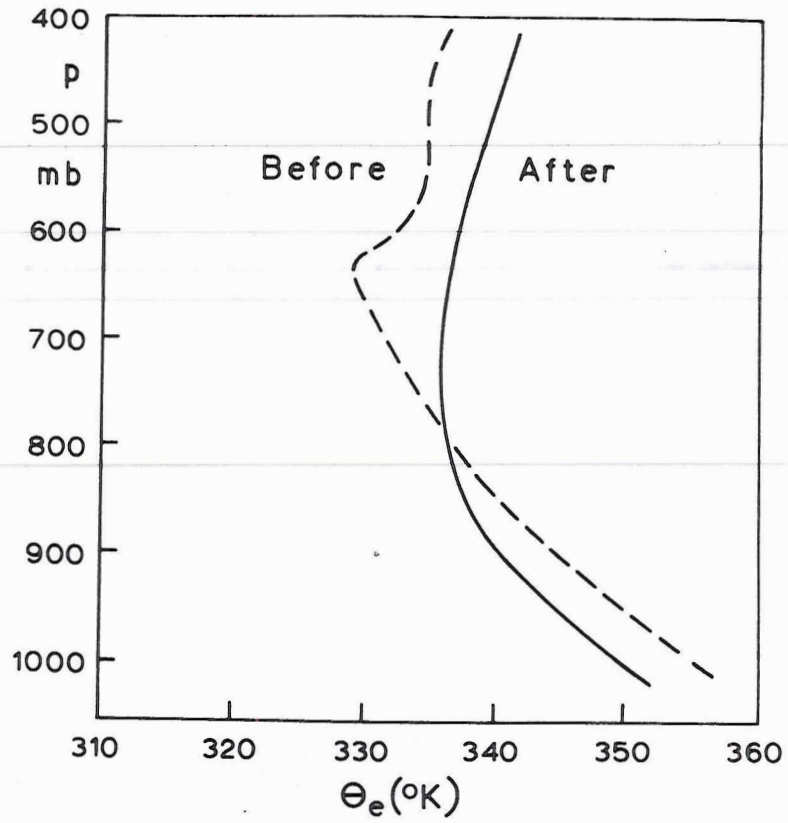


Fig. 6a. Profile of equivalent potential temperature against pressure at Guantanamo Bay before and after passage of the wave shown in Fig. 5a.

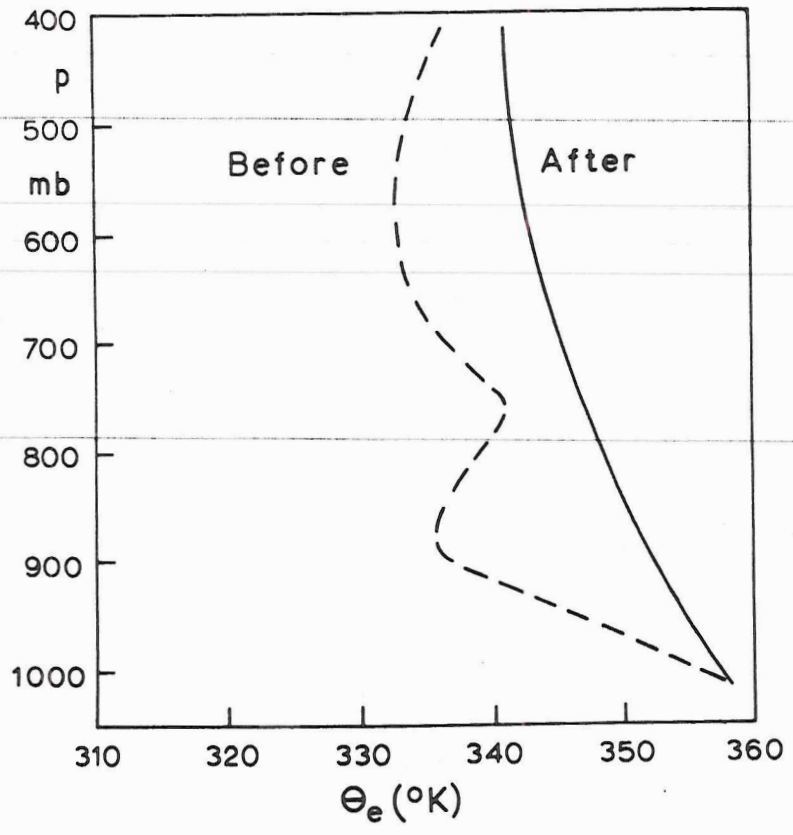


Fig. 6b. Profile of equivalent potential temperature against pressure at Kingston before and after passage of the wave shown in Fig. 5b.

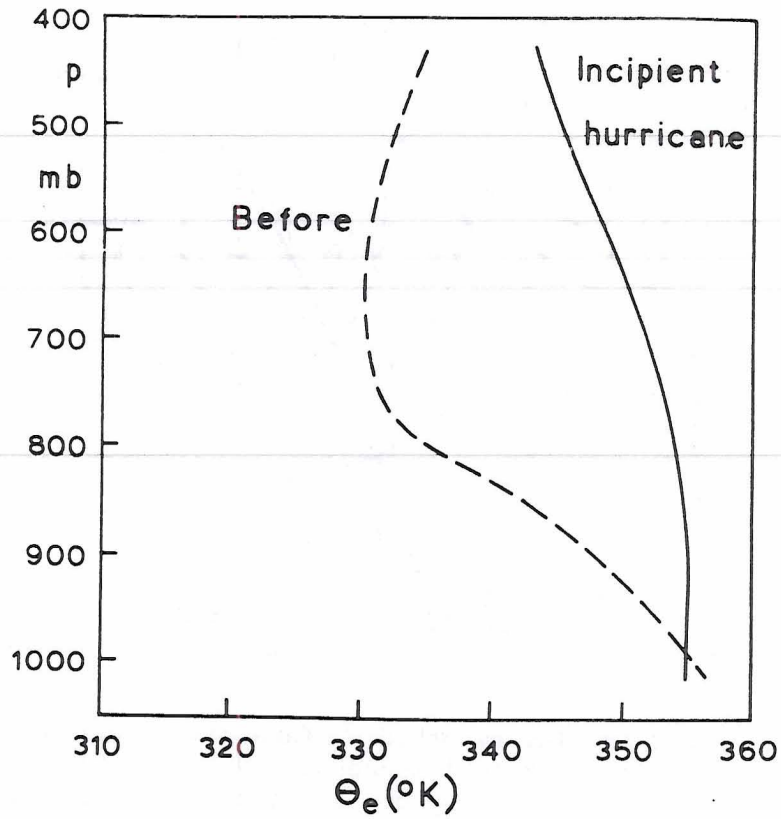


Fig. 6c. Profile of equivalent potential temperature against pressure at Gran Cayman on 3 October 1958 and at passage of incipient hurricane on 5 October 00 GMT.

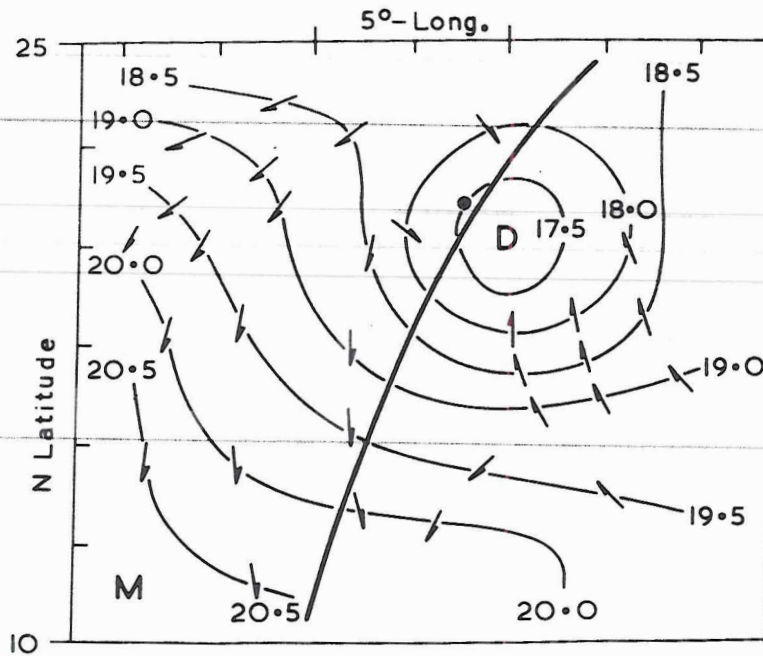


Fig. 7. Chart showing smoothed surface distribution of specific humidity (g/kg) 21 September 1959, 12 GMT. Heavy line is wave axis, heavy dot location of beginning hurricane center. Map extends from 10° to 25°N and has a 15° longitude interval centered on the wave axis in the west-central Caribbean. Arrows denote direction of relative motion streamlines at surface.

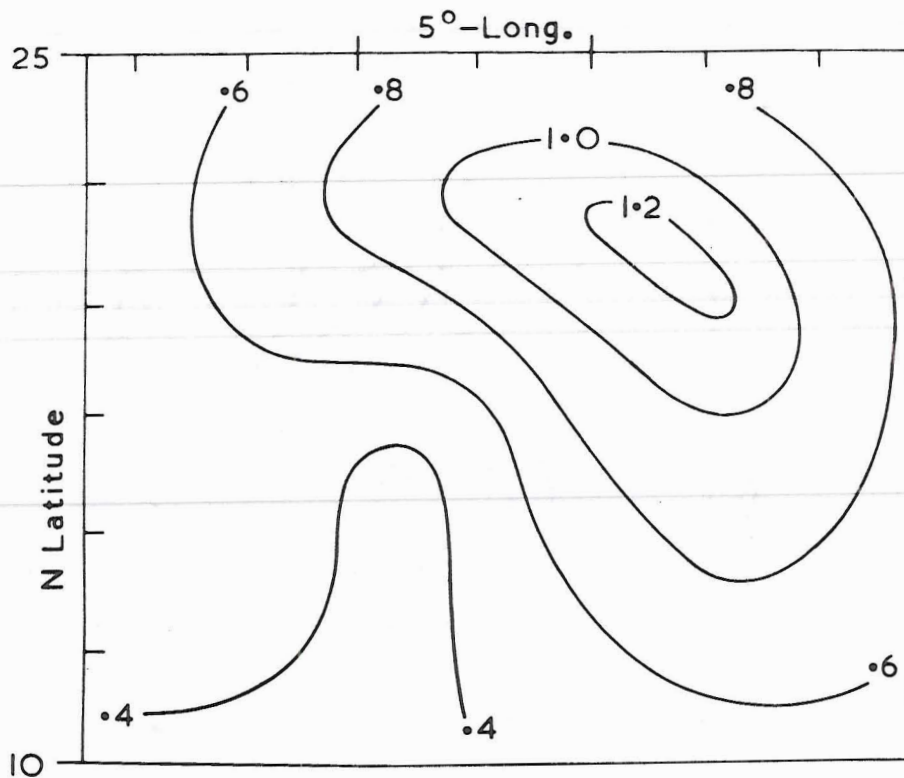
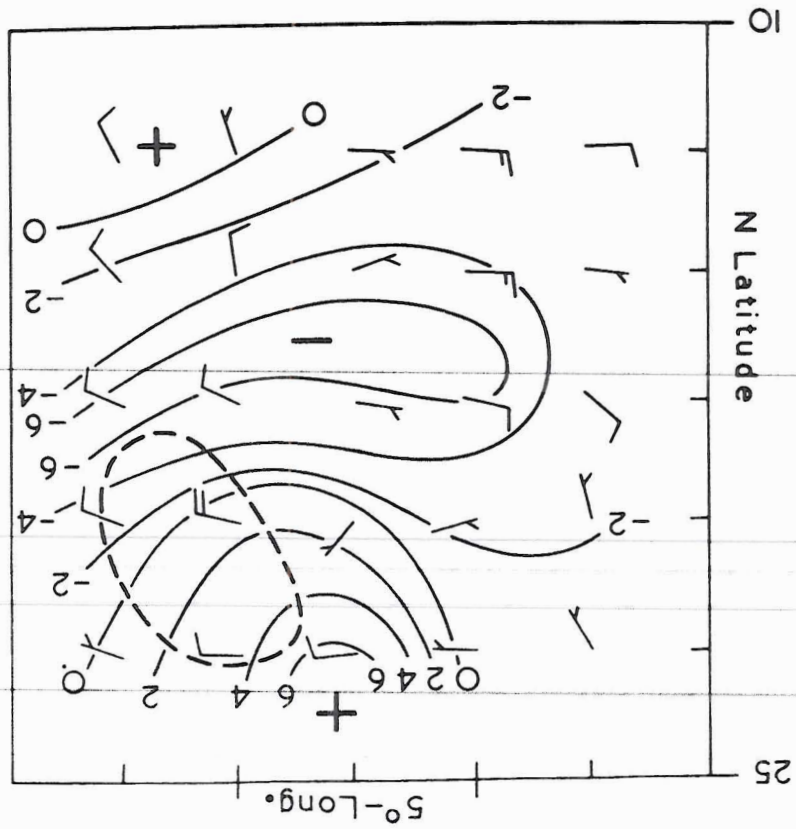


Fig. 8. Evaporation (cm/day), average for all cases. Map extends from 10° to 25°N and over 15 degrees longitude centered on each wave axis. Top of diagram shows 2.5°-longitude distance, which was basic distance of computational grid used.

Fig. 9. Energy loss or gain of surface air ( $10^{-6}$  cal/g/sec) and relative motion vectors at the surface, 15 September 1958. Map extent as in Fig. 8.



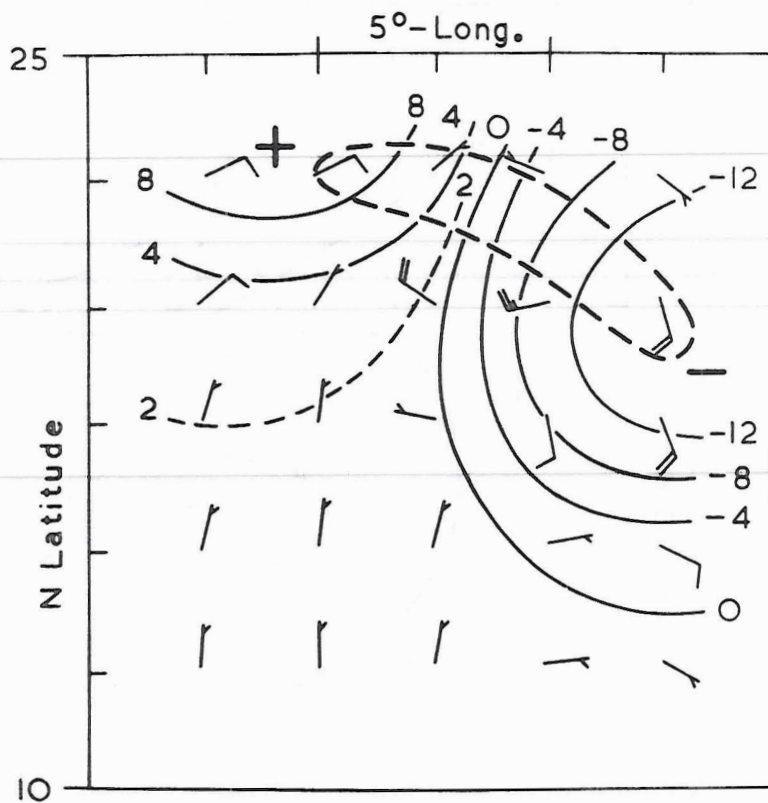


Fig. 10. Energy loss or gain of surface air ( $10^{-6}$  cal/g/sec) and relative motion vectors at surface, 21-22 September 1959.

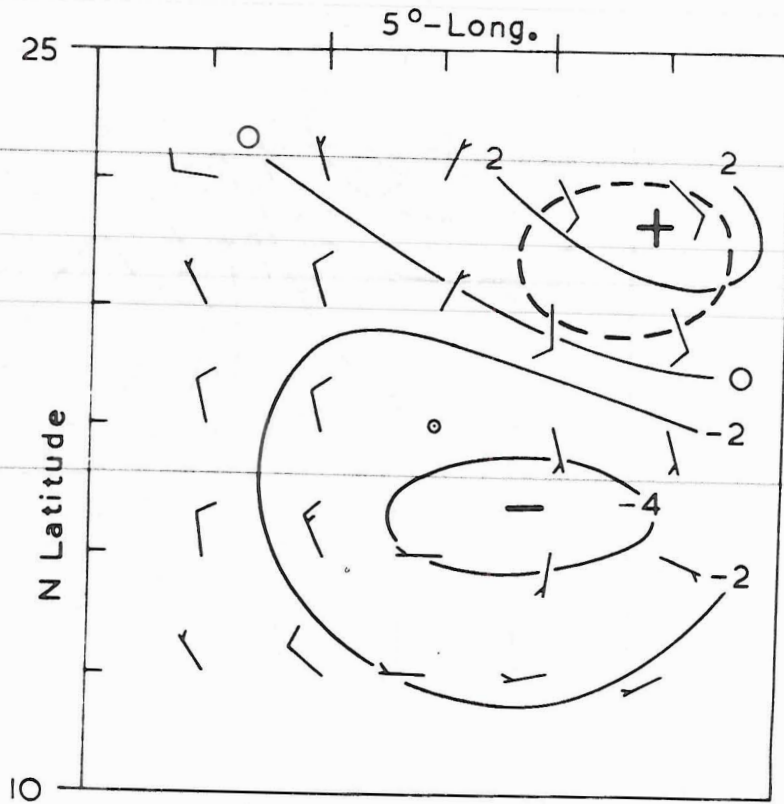


Fig. 11. Energy loss or gain of surface air ( $10^{-6}$  cal/g/sec) and relative motion vectors at surface, 7-8 August 1964.

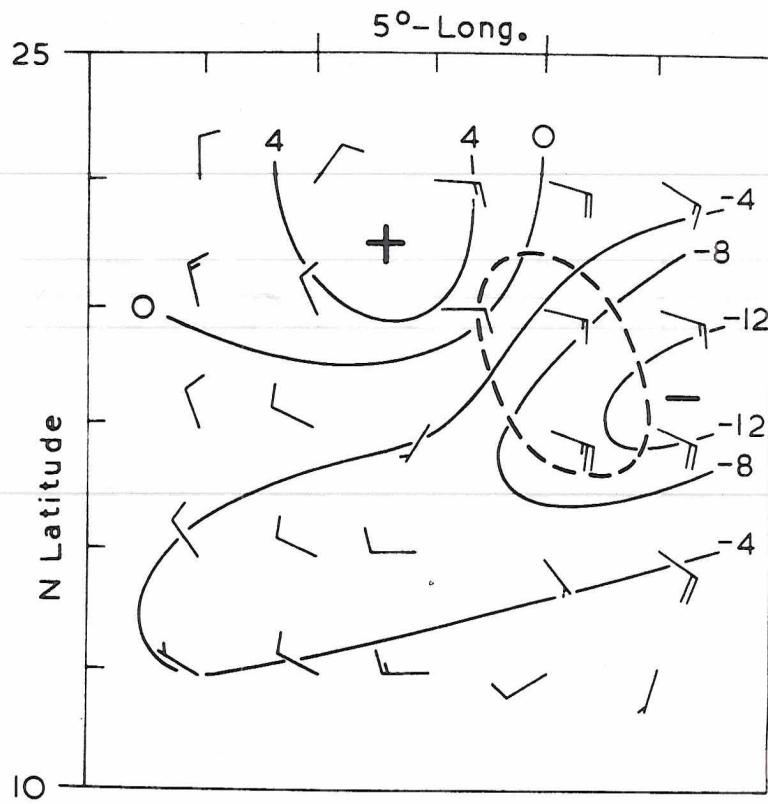


Fig. 12. Energy loss or gain of surface air ( $10^{-6}$  cal/g/sec) and relative motion vectors at surface, 13-14 September 1963.

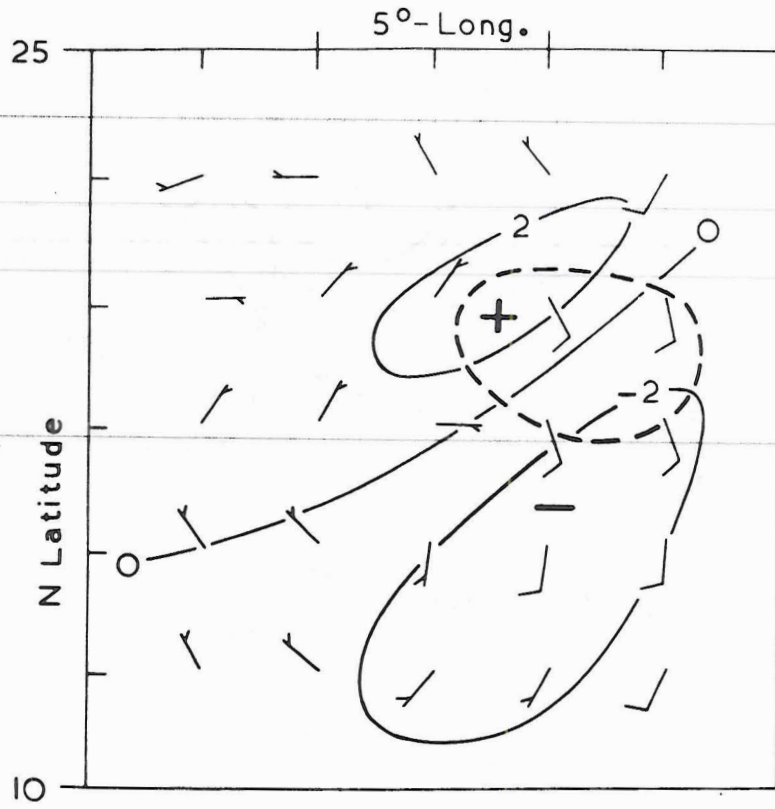


Fig. 13. Energy loss or gain of surface air ( $10^{-6}$  cal/g/sec) and relative motion vectors at the surface, 3-4 October 1958.

Part II  
VORTICITY BUDGETS DERIVED FROM CARIBBEAN DATA  
R.P. Pearce

Introduction

Perhaps the most important problem in tropical meteorology is that of determining the precise role of cumulus and cumulonimbus convection in the development and maintenance of larger-scale disturbances, such as Easterly waves. One of the main obstacles to progress is the scarcity of synoptic data. In an attempt to investigate the extent to which existing data can be used to make some progress with this problem, the five synoptic periods comprising fourteen map periods mentioned earlier, were selected for analysis in the Caribbean area. These constitute the best available data coverage to date over an area large enough to resolve a disturbance the size of a typical Easterly wave.

The data available was that obtained from radiosonde ascents together with observations from surface stations, including ships. Although it was at first hoped to be able to make use of all the reported upper air data, i.e. winds, dewpoints, temperatures and isobaric heights, the latter two were eventually discarded after several abortive attempts at smoothing. A typical example of the kind of height field reported at 200 mb is shown in Fig. 1. The work described here is an initial, purely kinematic analysis using the observed winds; this is to be extended to a heat budget analysis using the balance equation to derive the isobaric height and temperature fields. The wind data was subjectively analysed at each of the standard levels 1000, 850, 700, 500, 300, 200, and 150 mb by drawing streamlines and isotachs. The speeds and directions from N at points on a 7 x 7 isobaric grid (mesh length  $2\frac{1}{2}^{\circ}$  longitude, approximately 250 km) were read into a computer, which

calculated W-E and S-N components at each point. These components were then each smoothed in the vertical at each grid point to remove small vertical inconsistencies. The method used for this smoothing process, which enabled the main trends in the data to be preserved, is discussed in the next section.

Two methods for obtaining vertical velocities were tried initially. The first (A) is based on the vorticity equation

$$\frac{\partial \zeta}{\partial t} + \underline{v} \cdot \nabla \zeta + \omega \frac{\partial \zeta}{\partial p} = \zeta \frac{\partial \omega}{\partial p} \quad (1)$$

where  $\zeta$  is the absolute vorticity,  $\underline{v}$  the wind velocity and  $\nabla$  the gradient operator in an isobaric surface,  $p$  is the pressure,  $t$  the time and  $\omega = dp/dt$ . If convected coordinates are used (these coordinates having the property that, relative to them, the time derivatives of the system being analysed are associated only with changes of shape and not with propagation) then, if the convection velocity is  $\underline{v}_c$ , Eq. (1) may be written in the approximate form

$$\underline{v}_R \cdot \nabla \zeta + \omega \frac{\partial \zeta}{\partial p} = \zeta \frac{\partial \omega}{\partial p} \quad (2)$$

where  $\underline{v}_R = \underline{v} - \underline{v}_c$ . The wind field data yields  $\underline{v}_R$  and  $\zeta$  at the 6 x 6 grid of points interlacing the basic 7 x 7 grid and hence  $\underline{v}_R \cdot \nabla \zeta$  on the inner 5 x 5 network of basic points. Putting  $\omega = 0$  at  $p = p_0 = 1000$  mb (an approximation consistent with the use of convected coordinates) and integrating (2) then gives

$$\omega(p) = \zeta(p) \int_{p_0}^p \frac{\underline{v}_R \cdot \nabla \zeta}{\zeta^2} dp \quad (3)$$

The second method (B) was simply to integrate the continuity equation,

$$\nabla \cdot \underline{v}_R + \frac{\partial \omega}{\partial p} = 0 \quad (4)$$

giving

$$\omega(p) = \int_{p_0}^p - (\nabla \cdot \underline{v}_R) dp .$$

Method A has the advantage that vorticities are generally more accurately calculated than divergences (the components  $u_x$  and  $v_y$  of the latter usually having almost the same magnitude but opposite signs). On the other hand, method B is based on the continuity equation, which is virtually exact, whereas method A is based on the vorticity equation (2) which takes no account of vorticity changes associated with momentum transfer arising from the presence of subgrid scale convection. A more appropriate form of Eq. (2) applicable to situations in which these convection effects make an important contribution to the vorticity changes on the synoptic scale, as seems likely to be the case in the tropics, is

$$\frac{\partial \tilde{\zeta}}{\partial t} + \tilde{v}_R \cdot \nabla \tilde{\zeta} + \tilde{\omega} \frac{\partial \tilde{\zeta}}{\partial p} - \tilde{\zeta} \frac{\partial \tilde{\omega}}{\partial p} = - \tilde{v}_R' \cdot \nabla \tilde{\zeta}' - \tilde{\omega}' \frac{\partial \tilde{\zeta}'}{\partial p} + \tilde{\zeta}' \frac{\partial \tilde{\omega}'}{\partial p} + \tilde{\tau}' \quad (5)$$

where the tilde denotes an average in an isobaric surface over an area  $\Delta x \Delta y$ ,  $\Delta x$  and  $\Delta y$  being grid lengths in the W-E and S-N directions, and the prime denotes the local departure from the average.  $\tau'$  denotes the contribution from the twisting terms.

Since one aim of the analysis is to investigate how momentum transfer associated with subgrid scale convection might be incorporated into a numerical model of an Easterly wave, it is clear that using method A to estimate  $\tilde{\omega}$  can lead to no deductions concerning small-scale momentum transfer since this is implicitly assumed to be zero. It was therefore decided to attempt to refine method B and to use values of  $\tilde{\omega}$  deduced using Eq. (4) to estimate the relative magnitudes of the individual terms on the left hand side of Eq. (5) and the sum of those on the right hand side. If there should emerge consistent trends

over a number of map analyses, which is about all one could reasonably hope for in view of the errors in synoptic data, these trends would provide at least some indication of the importance of the contribution to the synoptic-scale vorticity field of effects described by the correlation terms on the right-hand side of Eq. (5). These results would then form a basis for a realistic parameterisation of these effects in terms of synoptic-scale quantities.

The results of this investigation are described and discussed below. The general trend of the correlation terms near the axes of the disturbances, whether they eventually develop into hurricanes or not, is towards reduction of the large-scale vorticity in the upper and lower troposphere and towards some increase of vorticity in the middle troposphere. The magnitude of these terms is the same as that of the terms on the left-hand side of Eq. (5).

The final part of the paper contains a discussion of the physical interpretation of these terms, leading to a reformulation of the vorticity equation in terms of the vorticity distribution inside cumulonimbus clouds, which is then estimated from the data.

#### Vertical Smoothing of the Data

Whereas horizontal consistency of wind data is ensured by the use of standard subjective analysis techniques applied at each standard pressure level, no attempt at vertical smoothing is attempted at the map analysis stage, i.e. the input data to the computer (wind speeds in kts and directions from N) is horizontally, but not vertically, smoothed. A technique for eliminating such vertical irregularities in the wind components, which does not suppress the main trends in the vertical profiles, was devised. This consists of approximating the data by fitting by least squares the piecewise continuous polynomial functions (spline functions) which seems to have been first suggested

by Fowler and Wilson (1962). The functional form used for the wind components was

$$\bar{u} = \begin{cases} u_0 + a_1q + a_2q^2 & , 0 \leq q \leq 5 \\ u_0 + a_1q + a_2q^2 + a_3(q-5)^2 & , 5 \leq q \leq 7 \\ u_0 + a_1q + a_2q^2 + a_3(q-5)^2 + a_4(q-7)^2 & , 7 \leq q \leq 8.5 \\ u_0 + a_1q + a_2q^2 + a_3(q-5)^2 + a_4(q-7)^2 + a_5(q-8.5)^2 & , 8.5 \leq q \leq 9 \end{cases} \quad (6)$$

where  $q = 10 - p/100$  with  $p$  in mb and  $a_1, a_2, a_3, a_4$  and  $a_5$  are parameters determined by the requirement that  $\sum_{i=1}^7 (\bar{u} - u_i)^2$  be a minimum; the summation is taken over the 7 data values at 850, 700, 500, 300, 200, 150 and 100 mb. (The components  $(u_0, v_0)$  at 1000 mb which were based on additional surface observations were assumed to be correct). The computer time involved in determining the parameters  $a_1$  to  $a_5$  for each vertical column is negligible if the matrix of their coefficients in the linear simultaneous equations they satisfy is inverted.

The piecewise defined function  $\bar{u}(q)$  is here chosen to be continuous and have a continuous first derivative at each of the 'joins' at  $q = 5, 7$  and  $8.5$ . These levels were chosen empirically, but with the purpose of enabling the best resolution of the data to be obtained at upper levels where maxima and minima tend to occur. The advantage of using such functions is that by suitably choosing the levels at which higher derivatives (in this case the second derivatives) change discontinuously, the meteorologically significant but sharp changes can still be preserved in some regions (for instance, near the tropopause) while, at the same time, overall gradual changes at other levels (e.g. up to 500 mb) are retained. It is not possible to do this, with the same number of parameters, if one tries to fit a function with all its derivatives continuous everywhere, such as, for instance, a quintic

polynomial. In a series of tests fitting polynomial and spline functions to isobaric height deviations from a standard tropical atmosphere, the root mean square deviations obtained using a spline function similar to the above were consistently about half those obtained using a quintic polynomial.

A typical set of components and their associated spline function is shown in Fig. 2. The effect of smoothing with the more conventional polynomial using the same number of parameters is also shown for comparison.

#### Computation of the $\omega$ -fields

Values of  $\partial u/\partial x + \partial v/\partial y$  are given by simple differences at the points forming a 6 x 6 grid interlacing the basic 7 x 7 grid. Averaging these values four at a time then yields estimates of the divergence at the inner 5 x 5 points of the basic grid. If these divergences are integrated through each column to estimate  $\omega$  (Eq. (4)) using simply the boundary condition

$$\omega = 0 \quad \text{at} \quad p = 1000 \text{ mb} \quad (7)$$

the  $\omega$ -fields at upper levels are highly unrealistic, particularly in the lower stratosphere where it is known that synoptic scale vertical motions rapidly decrease in amplitude. The constraint

$$\omega = 0 \quad \text{at} \quad p = 100 \text{ mb} \quad (8)$$

was therefore imposed in the numerical integration of Eq. (4) and incorporated into it by regarding the divergences at each level in each vertical column as data values subject to error. These were fitted by an approximating functional form. Again, trends were preserved as far as possible by using the spline function representation.

$$\nabla \cdot \underline{v} = \frac{\partial \bar{\omega}}{\partial q} = a_1 \{1 - 72H(q - 8.5)\} + a_2 \{2q - 648H(q - 8.5)\} \\ + a_3 \{2H(q-5) - 128H(q - 8.5)\} + a_4 \{2H(q - 8) - 8H(q - 8.5)\}$$

with

$$\bar{\omega} = a_1 \{q - 36H(q - 8.5)^2\} + a_2 \{q^2 - 324H(q - 8.5)^2\} \\ + a_3 \{H(q-5)^2 - 64H(q - 8.5)^2\} + a_4 \{H(q-8)^2 - 4H(q - 8.5)^2\}. \quad (8)$$

Here, the notation  $H(q - q_i)$  means

$$q - q_i, \quad q \geq q_i$$

$$0, \quad q \leq q_i$$

and  $H(q - q_i)^2$  means

$$(q - q_i)^2, \quad q \geq q_i$$

$$0, \quad q \leq q_i$$

(with acknowledgements to Heaviside).

Thus  $\bar{\omega}$ ,  $\frac{\partial \bar{\omega}}{\partial p}$  are continuous functions of  $p$  but  $\frac{\partial^2 \bar{\omega}}{\partial p^2}$  is discontinuous at 500, 200 and 150 mb;  $\bar{\omega}$  is zero at 1000 mb and at 100 mb. The parameters  $a_1$ ,  $a_2$ ,  $a_3$  and  $a_4$  are computed by solving the set of simultaneous equations (by matrix inversion) arising from the condition

that  $\sum_{i=1}^7 \left( \frac{\partial \bar{\omega}}{\partial q} - \nabla \cdot \underline{v}_i \right)^2$  should be a minimum.

A typical set of computed divergences and their associated spline function representation is shown in Fig. 3.

A typical  $\omega$ -field computed by this method is shown in Fig. 4. The relative wind distribution for this occasion and its associated vorticity field are shown in Figs. 5 and 6, and these are typical of most of the cases studied.

### The Computed Vorticity Budgets

The results for the five synoptic case studies are presented in Figs. 8-12. Each consists of two, three or four map periods and for each map period there are shown five vertical distributions. These distributions all refer to averages over the central 3 x 3 grid of basic points (approx.  $(750 \text{ km})^2$ ), across which the axis of the synoptic disturbance lies (the N-S edges of the 7 x 7 grid were varied from one map period to another to satisfy this requirement). The first vertical distribution shown for each map period is the absolute vorticity; the next three are, respectively, vertical inflow, large-scale generation and horizontal inflow of vorticity into unit vertical columns (shown schematically in Fig. 7). These quantities are plotted as a function of the pressure at the top of the column. They have been computed, respectively, as integrals with respect to  $p/g$  of the terms on the left-hand side of Eq. (5), i.e. the first three terms in the equation

$$\frac{\tilde{\omega}(p)}{g} \tilde{\zeta}(p) + \tilde{F}_0 + \int_p^{P_0} \tilde{\zeta} \frac{\partial \tilde{\omega}}{\partial p} \frac{dp}{g} - \int_p^{P_0} \nabla \cdot (\tilde{\mathbf{v}}_R \tilde{\zeta}) \frac{dp}{g} + X(p) = - \int_p^{P_0} R' \frac{dp}{g}. \quad (9)$$

Here the tilde denotes an average in an isobaric surface covering the central 3 x 3 grid of points;  $F_0$  is the flux of vorticity into the column associated with the surface boundary layer and has been computed from the empirical relation

$$F_0 = - c_D \rho_0 \left\{ \frac{\partial}{\partial y} (uV) - \frac{\partial}{\partial x} (vV) \right\} \quad (10)$$

where  $c_D$  is the drag coefficient (taken as  $1.5 \times 10^{-3}$ , the wind

components being in  $\text{ms}^{-1}$ ) and  $V^2 = u^2 + v^2 = \underline{v}^2$ ;  $R'$  denotes the terms on the right-hand side of Eq. (5). With the units used here, these integrated quantities may be regarded as contributing to twice the rate of change of angular momentum, in  $\text{gms}^{-1}$  per hour, of a unit column of section one square meter.

The integrals of the twisting terms omitted from the approximate vorticity equation (5), i.e.  $-\frac{\partial \tilde{v}}{\partial p} \frac{\partial \tilde{\omega}}{\partial x} - \frac{\partial \tilde{u}}{\partial p} \frac{\partial \tilde{\omega}}{\partial y}$  were also computed and found to be appreciably smaller than the other terms. These terms and  $-\partial_R \tilde{\zeta} / \partial t$  are denoted by  $X_{(p)}$  in Eq. (9) but computed values are not shown explicitly here.

The fifth of the sequences of five graphs in Figs. 8-12 represents the integral on the right-hand side of Eq. (9) i.e. the integrated rate of production of vorticity required to balance the sum of the four terms on the left-hand side. This is referred to as the small-scale generation rate. Reading across the last four graphs at any given pressure, the algebraic sum of the quantities represented is approximately zero, any differences from zero being attributable to the terms involved  $\partial_R \tilde{\zeta} / \partial t$  and the twisting effect.

The slopes of these last four graphs indicate the contributions to the vorticity budget of the unit column made by the individual layers of the atmosphere. Thus, where the upwards slope is to the right in the last of the five graphs, a small-scale generation of positive (cyclonic) vorticity at that level is implied; where it is upwards to the left, the implication is of small-scale generation of anticyclonic vorticity. The latter could alternatively be regarded as a reduction of cyclonic vorticity at the level considered. (One is tempted to use the term dissipation instead of reduction, but this is usually taken to imply that the process can be described in terms of a coefficient of eddy viscosity combined with derivatives of the mean field, and it is not intended to imply this interpretation here.)

## Discussion

### (a) Accuracy of Results

Clearly the errors in the analysis are dominated by errors in the  $\omega$ - and  $\zeta$ -fields. Although the  $\omega$ -fields are readily analysable at each pressure level and look encouragingly realistic (the quality of the fields reproduced in Fig. 4 is representative of the whole set), it would not be justifiable to regard individual grid-point values of  $\omega$  as being accurate to more than about  $\pm 3 \text{ mb hr}^{-1}$  at 700 and 300 mb and  $\pm 5 \text{ mb hr}^{-1}$  at 500 mb.

The implications of errors of this size on the accuracy of the computed small-scale vorticity generation rates can be roughly estimated as follows. It is first of all noticed that the mass divergence field has been balanced by computing the  $\tilde{\omega}$ -field using Eq. (4), and that, since  $\nabla \cdot \underline{v}$  has been assumed to vary linearly (piecewise) with  $p$ , no truncation errors have been introduced in the evaluation of the terms in Eq. (9) to upset this mass balance. Thus no errors in the residual are introduced through the sum of the components  $\tilde{\zeta} \partial \tilde{\omega} / \partial p$  (affecting the first term of Eq. (9)) and  $\tilde{\zeta} \nabla \cdot \underline{v}$  (affecting the third term), whatever the errors are in  $\tilde{\omega}$ .

Next it is seen that the sum of the first term (without  $F_0$ ) and the second in Eq. (9) is, on the whole, quite small compared with their individual values. This is to be expected, since the sum is

$$\int_p^{p_0} \tilde{\omega} \frac{\partial \tilde{\zeta}}{\partial p} \frac{dp}{g}, \text{ i.e. the integral of the rate of vertical advection of}$$

vorticity, which is well-known to be small compared with the horizontal advection rate on the synoptic scale. Except at levels above 500 mb,  $\partial \tilde{\zeta} / \partial p$  is usually very small, as indicated by the first of the graphs, so that errors in  $\tilde{\omega}$  cannot affect the residual very much through this term. Taking, for instance,

$\frac{\partial \tilde{\zeta}}{\partial p} = 0.3 \times 10^{-5} \text{ s}^{-1} (100 \text{ mb})^{-1}$ ,  $\delta \tilde{\omega} = 2 \text{ mb hr}^{-1}$  (the error in  $\tilde{\omega}$  averaged over 9 grid-points assumed the same at all levels), the error in the integrated small-scale generation rate at 200 mb is -0.48 units; at 500 mb it is -0.30 units.

The main effect of errors in  $\tilde{\omega}$  is therefore through the component

$-\int_p^{p_0} \tilde{\zeta} \cdot \nabla_{\underline{v}_R} \frac{d\tilde{\omega}}{g}$  of the third term in Eq. 9. This is simply the same as the second term, i.e.  $\int_p^{p_0} \tilde{\zeta} \frac{\partial \tilde{\omega}}{\partial p} \frac{dp}{g}$ . With  $\delta \tilde{\omega} = 3 \text{ mb hr}^{-1}$

at 500 mb,  $\tilde{\zeta} = 5 \times 10^{-5} \text{ s}^{-1}$ , the error in the integrated small-scale generation rate at 500 mb is -1.5 units; it decreases above and below this level.

The other source of error is the component  $-\int_p^{p_0} \underline{v}_R \cdot \nabla \tilde{\zeta} dp/g$  of the third term in Eq. (9). With  $\underline{v}_R$  of magnitude  $15 \text{ ms}^{-1}$  and  $\nabla \tilde{\zeta}$  in error by  $f$  per 500 km, the error in the small-scale generation rate at 500 mb due to this term is of magnitude 3 units.

These estimates of likely extreme values of error suggest that the estimates of small-scale generation rates of vorticity for individual occasions in Figs. 8-12 should be regarded as subject to errors of magnitude of about  $\pm 5$  units. It is therefore possible to draw conclusions from such estimates only on the basis of statistically significant trends, and conclusions drawn from the present small sample of occasions can strictly only be regarded as tentative.

(b) The Five Synoptic Periods

These are first of all considered separately. A feature of all the results in Figs. 8-12 which is worth bearing in mind, however, is that the values of vertical inflow of vorticity almost offset the values of the large-scale generation rate at each level (second and third graphs) and that the values of small-scale generation rate almost offset those of the horizontal inflow. This is in accordance with the conclusions of the analysis in the last section. Also, since  $\tilde{\zeta}$  does not alter in size with height, the integrated vertical inflow curve (second graph, ignoring  $F_0$ ) closely resembles the curve of  $\tilde{\omega}$ ; 4 units can be regarded as representing approximately  $8 \text{ mb hr}^{-1}$ .

To understand the orders of magnitude of the changes being discussed, it is worth noting that twice the absolute angular velocity of an atmospheric column of cross section one  $\text{m}^2$  extending from the surface to 500 mb is approximately  $250 \text{ gm s}^{-1}$  (taking  $\zeta = 5 \times 10^{-5} \text{ s}^{-1}$ ). A value of  $2.5 \text{ gm s}^{-1} \text{ hr}^{-1} \text{ m}^{-2}$  at 500 mb of any of the quantities represented in the last four graphs in Figs. 8-12 thus represents an increase of twice the absolute angular velocity of the column up to 500 mb of 1% per hour.

Case 1, 7-8 August 1964: A 'cold-core' disturbance progressed steadily westwards across the Caribbean at about  $8-10 \text{ ms}^{-1}$ . The disturbance maintained a relatively steady state and there was no sign of the formation of a hurricane vortex. The computed fields at 7 August 0000 and 8 August 0000 are broadly similar, but the one at 7 August 1200 shows only small vertical motions. These differences are presumably indicative of error in the analysis. All three cases show an overall reduction of vorticity due to sub-grid scale convection, most of this occurring at lower and upper levels. At middle levels there is some evidence of vorticity increase associated with convection effects.

Case 2, 15 September 1958: This was another steady-state disturbance, slightly cold-core below 500 mb, but with a strong outflow anticyclone at 200 mb. This system progressed steadily westwards at about  $9 \text{ ms}^{-1}$  without developing a hurricane vortex, although at one stage there was evidence of a closed circulation on the surface chart and a reconnaissance mission was sent out to the area south of Hispanola.  $\tilde{\zeta}/\partial p$  is larger here than in Case 1 and increased slightly over the 12-hour period shown. To balance the vorticity budget it is necessary to invoke a large rate of reduction of vorticity associated with sub-grid scale effects at all levels.

Case 3, 3-5 October 1958: This was an occasion on which a hurricane vortex formed near the center of the region towards the end of the period studied, the Easterly wave progressing westwards at  $8 \text{ ms}^{-1}$  and slowing down. The average vorticity over the region is seen to increase below 500 mb and decrease somewhat at upper levels during the last 12-hour period shown. All four analyses show average ascending motion over the region (second graph). Also, all four graphs show a reduction of vorticity associated with small-scale effects in the layer below 700 mb and, apart from the last of the map periods, an increase in the middle layers. The last two indicate a further reduction at upper levels, a pronounced effect in the last case.

Case 4, 21-22 September 1959: This wave, moving westward at  $9 \text{ ms}^{-1}$ , after several abortive attempts eventually developed into a hurricane vortex in the NE quadrant of the 7 x 7 grid at the end of the period studied. The central area of the grid does not therefore cover the main region of development and this is perhaps why all the distributions shown are rather weak. It is interesting that the basic graph for the last map period when the vortex had formed shows a large reduction of vorticity at upper levels similar to that in the corresponding graph in Case 3.

Case 5, 13-14 September 1963: This was the rather exceptional 'warm core' wave previously studied by Elsberry (1965). Its fundamentally different dynamical structure from the other four cases is reflected in the first graph, showing an increasing absolute vorticity at upper levels with a well marked minimum at 500 mb. Also the levels above 500 mb are subsiding (second graph) over the slightly ascending lower troposphere i.e. there is horizontal divergence in the middle troposphere associated with convergence both above and below. It is therefore unlikely that convective activity extended above 500 mb and cloud reports indicate that this was the case. This example can be regarded as a test of the method of analysis, since with no convective activity above 500 mb the last of the graphs should both be parallel to the pressure axis above 500 mb. Before the twisting terms were computed both showed an upward slope towards the right of about the same magnitude as the lower slope to the left, indicating small-scale vorticity generation; inclusion of the twisting terms has still left a slope to the right which must be attributed to error. Below 500 mb the curves suggested a reduction of vorticity associated with sub-grid scale convection.

(c) Physical Interpretation

It has been suggested by several authors (e.g. Riehl and Malkus, 1958) that the ascent of air associated with synoptic-scale low-level convergence and high-level divergence in the tropics takes place almost entirely in cumulonimbus (so-called hot towers) and that the bulk of the air at middle levels, i.e. in the clear air between the cumulonimbus, does not ascend and may, indeed, be slowly descending. This physical picture implies that negative  $\bar{\omega}$  fields, computed from synoptic-scale horizontal divergences, indicate, not large-scale regions of ascent, but differences of concentration of cumulonimbus; when this concentration is large in a given grid square compared with the surrounding grid squares a net lower level convergence and upper

level divergence into the central grid square is observed. This is clear if one considers, for instance, a 3 x 3 group of adjacent grid squares, the inner one having  $n + m$  hot towers and the other eight each having  $n$ . Suppose that the density of  $n$  cumulonimbus per grid square extends in all directions outwards from the region considered. Then there must be a net lower level convergence and upper level divergence into the inner grid square associated with the  $m$  extra cumulonimbus it contains. The opposite occurs if  $m$  is negative. As a numerical example, suppose  $n = 20$  per grid square of side 250 km i.e. the cumulonimbus are generally about 60 km apart, whereas in the central square they are 30 km apart i.e.  $m = 60$ . Further suppose that the ascending towers have an average cross section of 3 sq km at 500 mb and rise, on average, at  $10 \text{ ms}^{-1}$ , i.e. approximately  $2000 \text{ mb hr}^{-1}$ . Assuming that all the clear air at this level is at rest, since the rising towers occupy 0.3% of the area,  $\bar{\omega} = 6 \text{ mb hr}^{-1}$ . The  $\omega'$  field (Eq. 5) thus has very large values of approximately  $300 \bar{\omega}$  in the cumulonimbus towers and a value of about  $-\bar{\omega}$  in the clear air.

To understand the implications of this distribution of vertical velocity and the associated divergence and vorticity as they affect the vorticity budget computation carried out above, it is convenient first to consider the consequences of integrating the horizontal momentum equation in the form

$$\frac{\partial \underline{v}}{\partial t} + \nabla (gh + \frac{\underline{v}^2}{2}) - \underline{v} \times \underline{\zeta} + \omega \frac{\partial \underline{v}}{\partial p} = 0, \quad (11)$$

taking its tangential component, round a contour in an isobaric surface (height  $h$ ) surrounding a single representative cumulonimbus cell containing a central updraught surrounded by a descending environment (see Fig. 13 for the flow envisaged in a vertical section through the axis of such a cell). If  $\zeta_e$  and  $\omega_e$  denote values of  $\zeta$  and  $\omega$  representative of the boundary, and  $c$  and  $d$  denote respectively the circulation and divergence at the boundary, this integration yields

$$\frac{\partial c}{\partial t} + \omega_e \frac{\partial c}{\partial p} + \zeta_e d = 0 , \quad (12)$$

which is a form of the circulation theorem. (The same result is obtained if the vorticity equation, written in the form

$$\frac{\partial \zeta}{\partial t} + \nabla \cdot (\underline{v}\zeta - \omega \underline{\zeta}_h) = 0 ,$$

which includes the twisting terms, is integrated over the area contained by the contour).

If a grid square is regarded as comprising a number (n, say) of such representative cells, packed without any gaps between them, such an integration round each cell is equivalent to integration round the grid square, and Eq. (12) becomes

$$\frac{\partial C}{\partial t} + \omega_e \frac{\partial C}{\partial p} + \zeta_e D = 0 \quad (13)$$

where C and D denote, respectively, the circulation and divergence round the boundary of the grid square. Dividing Eq. (13) by the area of the grid square gives

$$\frac{\partial \tilde{\zeta}}{\partial t} + \omega_e \frac{\partial \tilde{\zeta}}{\partial p} + \zeta_e \tilde{D} = 0 \quad (14)$$

where

$$\tilde{D} = - \frac{\partial \omega}{\partial p} . \quad (15)$$

This, therefore, is the form of the vorticity equation which is appropriate to describe a cumulonimbus population, rather than Eq. (1) with

$\zeta$ ,  $\underline{v}$  and  $\omega$  taken as  $\tilde{\zeta}$ ,  $\tilde{v}$  and  $\tilde{\omega}$ . The differences between the two formulations arise from (a) including the twisting terms, which are important on the scale of the cumulonimbus since  $\nabla\omega$  is locally large and (b) distinguishing clearly between  $\tilde{\omega}$  and  $\tilde{\zeta}$  on the one hand and  $\omega_e$  and  $\zeta_e$  on the other. For the flows indicated in Fig. 13,  $\omega_e$  is positive, whereas the net lower level convergence and upper level divergence imply that  $\tilde{\omega}$  is negative. It is reasonable to expect  $\zeta_e$  to be smaller than  $\tilde{\zeta}$ , at least in the lower layers, since, as has been pointed out above, convergence must concentrate the vorticity at the storm axis.

If the computed residuals are now examined qualitatively in the light of this new formulation, restricting consideration to cases 1, 2 and 3, which are the only ones with  $\tilde{\omega} < 0$  through most of the troposphere, the feature mentioned above, that the residual values largely offset the horizontal inflow values, becomes highly significant. It suggests that the horizontal inflow values have been much overestimated as a result of treating the last term in Eq. (14) effectively as  $\tilde{\zeta}D$  instead of  $\zeta_e D$  i.e. the residuals suggest that  $\zeta_e/\tilde{\zeta}$  could be quite small.

This qualitative interpretation of the results suggested that the computed residual should be used to estimate  $\zeta_e$  values consistent with Eq. (14), for some assumed values of  $\omega_e$ . Such a computation has been carried out on a desk calculator, it being assumed, for convenience, that

$$\omega_e = -n_1 \tilde{\omega} \quad (16)$$

$$\zeta_e = n_2 \tilde{\zeta} \quad (17)$$

where  $n_1$ ,  $n_2$  are constants. The formula used for this purpose was

$$\tilde{\zeta}_e = \tilde{\zeta} - \frac{g}{\Delta\omega} \left[ \Delta \left\{ I + (n_1 - 1) I' \right\} - \frac{\Delta p}{g} \frac{\partial \tilde{\zeta}}{\partial t} \right] \quad (18)$$

where  $gI = \int_p^{p_0} R' dp$  and  $gI' = \int_p^{p_0} \tilde{\zeta} \frac{\partial \omega}{\partial p} dp - \tilde{\omega} \tilde{\zeta}$ , both of these

quantities being available as computer output. ( $\Delta$  denotes a finite difference operator. At middle levels where  $\Delta\omega$  is small, ratios of second differences were used.)

Values of  $\zeta_e/\tilde{\zeta}$  ( $= n_2(p)$ ) for each layer of the atmosphere were tabulated for  $n_1 = 0, 1$  and  $2$  using Eq. 18. These layer values were then averaged, weighted according to layer thickness, to give representative values of  $n_2$  for the whole atmosphere. Since, for each layer, Eq. 18 (with  $\zeta_e$  put equal to  $n_2 \tilde{\zeta}$ ) is linear in  $n_1$  and  $n_2(p)$ ,  $n_2$ , the average value, is a linear function of  $n_1$ .

Figure 14 shows  $n_2$  (for the range  $0 \leq n_2 \leq 1$ ) as a function of  $n_1$  for the eight occasions analysed. All the lines slope downwards to the right, which implies that the more rapidly the clear air is assumed to subside, the smaller becomes the value of  $\zeta_e/\tilde{\zeta}$  required to balance the vorticity equation (Eq. 14) in each case. There are one or two cases which look unrealistic, notably that for 0000, 4.10.58 which looks too small, but on the whole, the results lend strong support to the theoretical analysis suggested above and suggest that the clear air between the cumulonimbus clouds subsides at a rate of about  $10 \text{ mb hr}^{-1}$ .

It must be emphasised that this analysis is a purely kinematic one. The above conclusions may need to be modified when the thermodynamics of the cumulonimbus clouds and their environment is considered. For instance, the value of  $10 \text{ mb hr}^{-1}$  quoted above as a likely one for  $\omega_e$  in the middle troposphere would require a heat sink capable of producing a rate of cooling of the air of about  $8^\circ\text{C}$  per day which is about ten times the average radiative value, and this could prove to be unrealistic. It

could be the case, however, that evaporative cooling effects make an important contribution towards maintaining the environmental heat balance and would, if taken into account, support the value of  $\omega_e$  suggested here.

(d) Modification of the Large Scale Vorticity Field by Cumulonimbus

If it is accepted that the vorticity field measured on a synoptic grid in the tropics may be regarded as representing a population of cumulonimbus circulations of the type shown in Fig. 13, it is possible to deduce some characteristics of this field. Suppose that, initially, the vorticity is of a constance value  $\tilde{\zeta}$  at all levels in a given grid area and suppose that cumulonimbus activity then commences, each cell contributing its portion of the net low level convergence and upper level divergence of mass. Eq. (14) applies initially with  $\zeta_e = \tilde{\zeta}$  and  $\frac{\partial \tilde{\zeta}}{\partial p} = 0$  and it is clear that  $\tilde{\zeta}$  drops at upper levels and increases at a similar rate at lower levels, by mass continuity. Thus  $\frac{\partial \tilde{\zeta}}{\partial p}$  becomes positive. As long as  $\zeta_e$  is reasonably approximated by  $\tilde{\zeta}$ , there is rather more horizontal inflow of vorticity than outflow, but this apparent net increase of total vorticity (in the volume defined by the grid and the depths of the troposphere) is offset by the  $\omega_e \frac{\partial \tilde{\zeta}}{\partial p}$  term which, with  $\omega_e > 0$ , soon acts to decrease the total vorticity. As the convection proceeds and  $\zeta_e$  becomes smaller (which seems a reasonable assumption), if it is assumed that the  $\omega_e$  term dominates, then there is a net reduction of total vorticity in the volume, a compensating increase occurring externally. More formally, integration of Fig. 14 through the depths of the atmosphere gives  $\frac{\partial \tilde{\zeta}}{\partial t} = (n_1 - n_2) \int \tilde{D} \tilde{\zeta} dp/g$ , which is negative with typical  $\tilde{D}$  and  $\tilde{\zeta}$  profiles and  $n_1 - n_2 > 0$ .

Scorer (1965) has proposed that anvil spreading combined with smaller scale mixing tends to redistribute the momentum so as to reduce the absolute vorticity in the body of the fluid and concentrate it at the boundaries or in the middle of the stirred region. This proposition is based on the general principle that the stirring will make a rotating

fluid which is initially in a dynamically stable state tend to become more nearly neutral i.e. more like a potential vortex. Scorer strongly emphasises the importance of mixing on a scale smaller than that of the cumulonimbus to make this process effective since he requires the 'displaced parcels' to mix with their environment. The treatment suggested here, which regards the whole grid area as consisting of cumulonimbus 'cells', each cell containing the updraught and a large area of down-draught, seem to be capable of producing a horizontal (and vertical) redistribution of vorticity without invoking smaller scale mixing. The essential feature is the dynamical structure of the cumulonimbus itself, and the concept of an 'environment' with which it 'mixes' does not seem appropriate; all that is required is a concentrated updraught surrounded by a compensating downdraught distributed over a much larger area.

(e) The Balance Equation

The above interpretation of the synoptic scale wind fields associated with cumulonimbus populations implies modification, not only of the vorticity equation, but also of the balance equation relating the pressure and wind fields. If the component of Eq. (11) normal to a contour in an isobaric surface surrounding a single cumulonimbus cell of area A is integrated round the contour, the resulting equation, after dividing by A, is

$$\frac{1}{A} \oint \nabla_n \Psi \, dl = \zeta_e (\tilde{\zeta} - f) - \frac{\partial \tilde{D}}{\partial t} - \omega_e \frac{\partial \tilde{D}}{\partial p} \quad (19)$$

where

$$\Psi = gh + \frac{1}{2} \underline{v}^2 \quad (20)$$

The term on the left may be interpreted as  $\nabla^2 (gh_o + \frac{1}{2} v_o^{*2})$  where suffix o denotes a value representative of a cumulonimbus cell at the

centre of the grid area (i.e. not an average over the whole grid area) and  $v^{*2} = \bar{v}^2$ . In view of the large departures of  $\underline{v}$  from  $\bar{v}$ , at least at upper and lower levels, one would expect  $v^{*2}$  to be larger than  $\bar{v}^2$ , perhaps by as much as 50%.

Thus it is necessary to postulate  $\zeta_e$ ,  $\omega_e$  and  $v^{*2}$  in order to derive the pressure field corresponding to a given wind field associated with a cumulonimbus population.

### Conclusion

The above purely kinematic analysis of the observations was developed as a consequence of abandoning the temperature and height data, and it probably approaches the limit of refinement possible using conventional wind data on the present Caribbean station network. It was only after the vorticity budgets (Figs. 8-12) had been obtained and their implications studied that the theory leading to Eq. (14) was developed and the further computations leading to the results Fig. 14 carried out.

It is therefore perhaps encouraging to find that conventional wind observations in the tropics, when analysed with sufficient care, produce results which are sufficiently coherent to suggest a dynamical structure for tropical disturbances, even through individual basic elements of this structure, the cumulonimbus, are not resolved by the observation network.

## References

- Elsberry, R., 1965: On the mechanics and thermodynamics of a low-level wave in the easterlies. Dept. Atmos. Sci., Colo. State Univ., Fort Collins, Colo. 31 pp, mimeographed.
- Fowler, A.H. and C.W. Wilson, 1962: Cubic spline, a curve fitting routine. Report No. Y-1400, Oak Ridge National Laboratory.
- Riehl, H. and J.S. Malkus, 1958: On the heat balance in the equatorial trough zone. Geophysica, Helsinki, 6, p. 503.

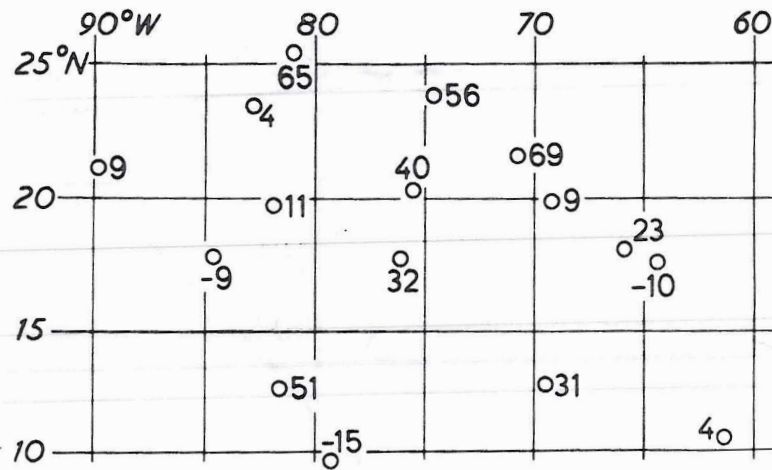


Fig. 1. Observed 200 mb height deviations (in meters) from standard tropical atmosphere value of 12396 m, 15.9.58, 0000.

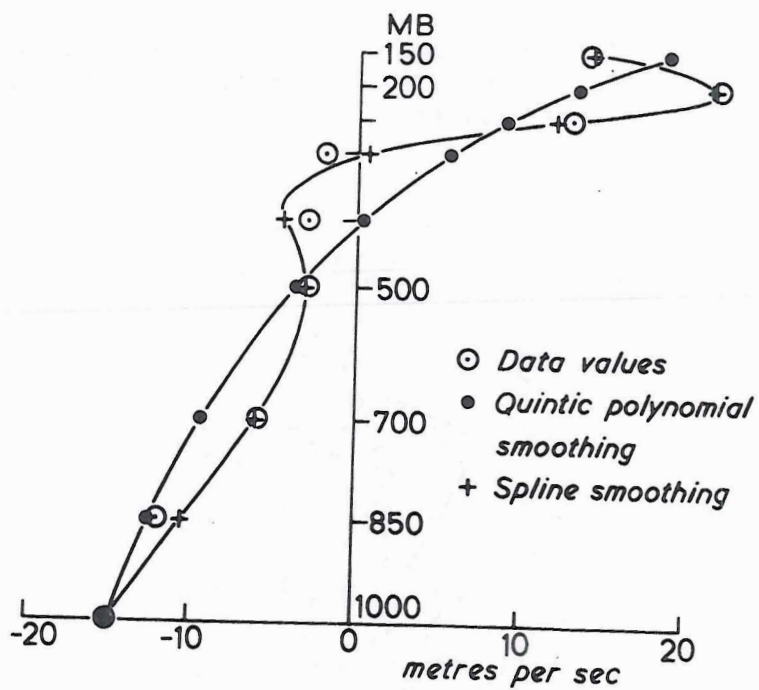


Fig. 2. Smoothing of wind components.

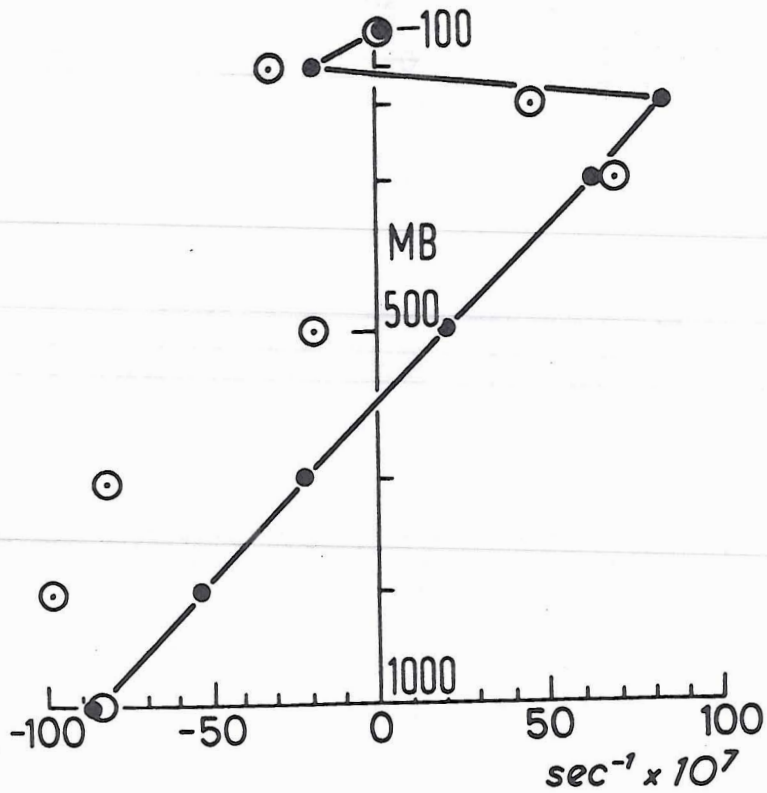


Fig. 3. Spline smoothing of horizontal divergences 21.9.59, 0000. 15°N, 75°W. ⊙ computed divergences, • spline smoothed values.

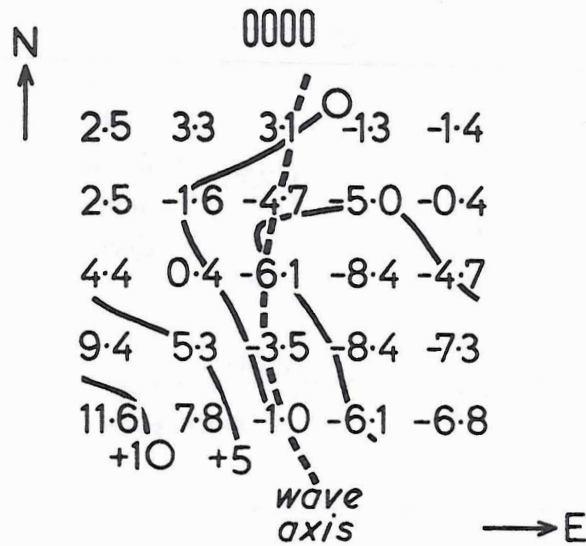


Fig. 4. Computed 500 mb  $\tilde{\omega}$ -field in  $\text{mb hr}^{-1}$  4.10.58, 0000.

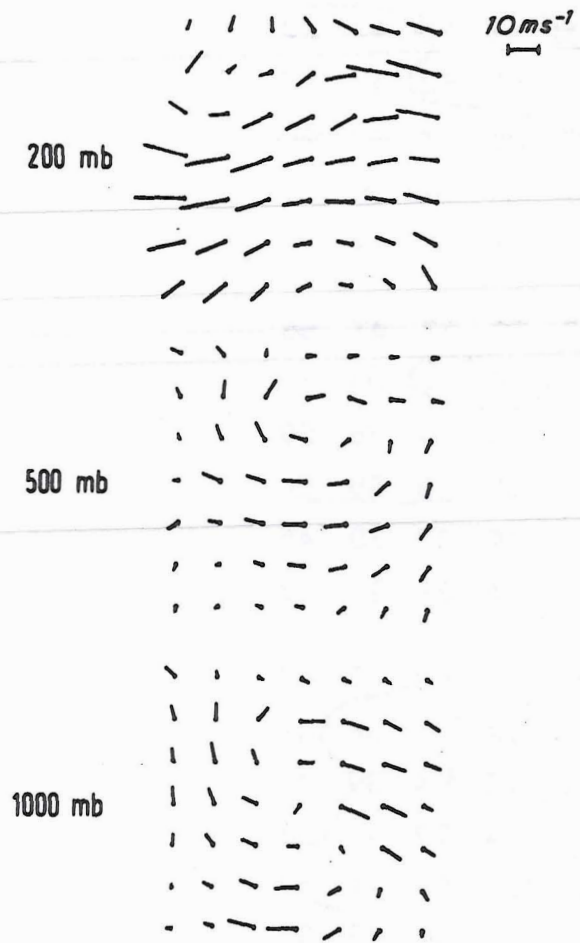


Fig. 5. Relative winds 4.10.58, 0000.

200 mb

57	70	83	68	73	84
113	102	83	50	22	24
104	86	59	52	44	23
74	49	28	33	42	40
29	17	9	16	18	15
15	13	11	15	14	4

500 mb

43	52	59	53	47	56
46	72	114	115	85	76
50	63	75	74	76	59
32	40	50	48	58	58
18	18	29	37	38	45
25	24	24	27	21	28

1000 mb

57	66	58	44	43	47
52	76	92	76	58	49
48	68	90	64	39	48
44	56	64	77	71	37
36	37	56	61	71	57
33	35	58	56	42	37

Fig. 6. Absolute vorticity fields in units  $\text{sec}^{-1} \times 10^{-6}$  4.10.58, 0000.

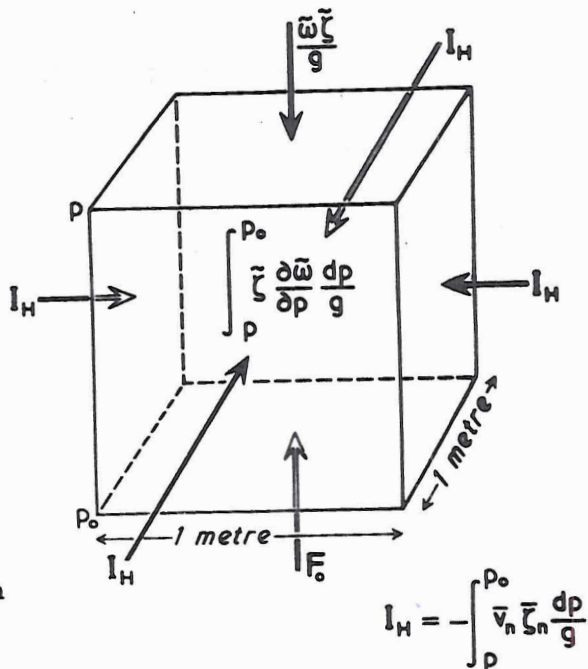


Fig. 7. Schematic representation of terms in Eq. (9).

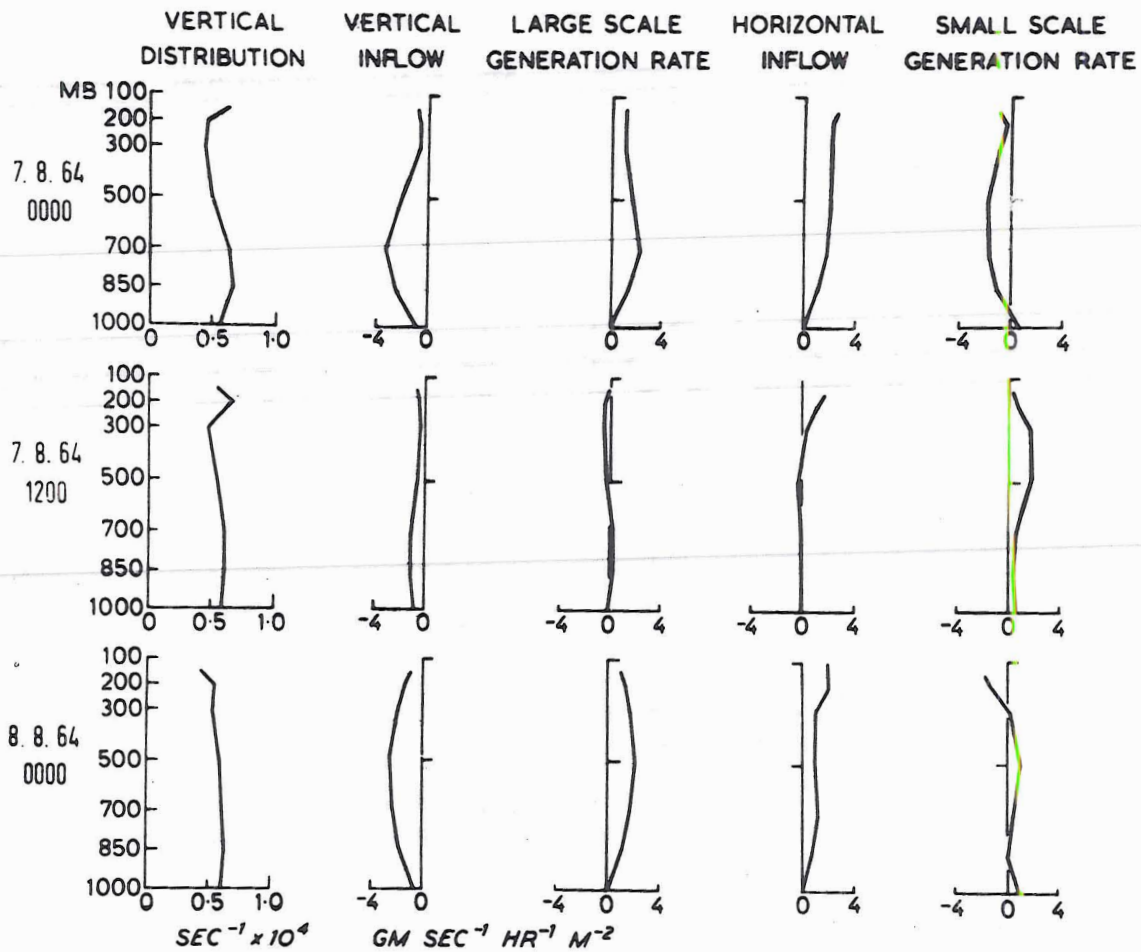


Fig. 8. Vorticity analysis. Case 1. 7-8 Aug. 1964. Non-developing cold-core wave moving westward at  $8 \text{ ms}^{-1}$ .

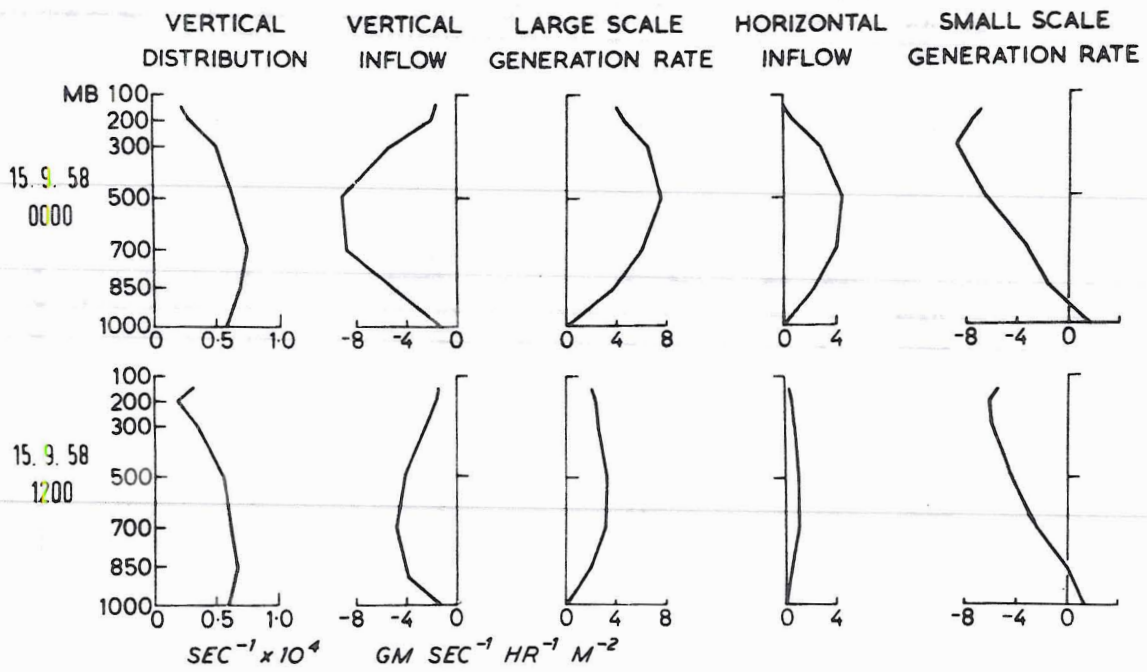


Fig. 9. Vorticity analysis. Case 2. 15 Sept. 1958. Cold-core wave with abortive vortex moving westward at  $9 \text{ ms}^{-1}$ .

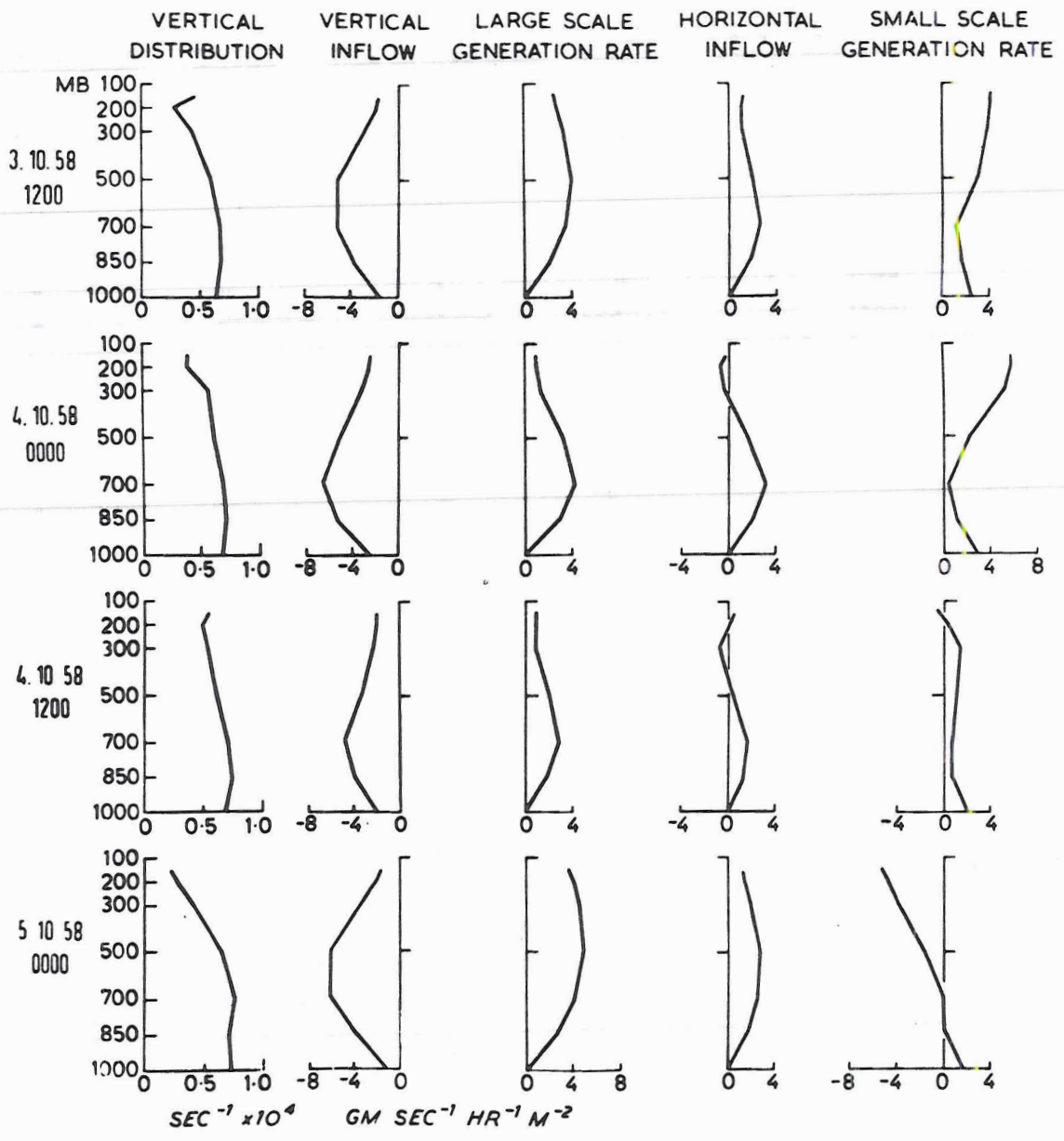


Fig. 10. Vorticity analysis. Case 3. 3-5 Oct. 1958. Wave moving westward at  $6 \text{ ms}^{-1}$  developing rapidly into a hurricane.

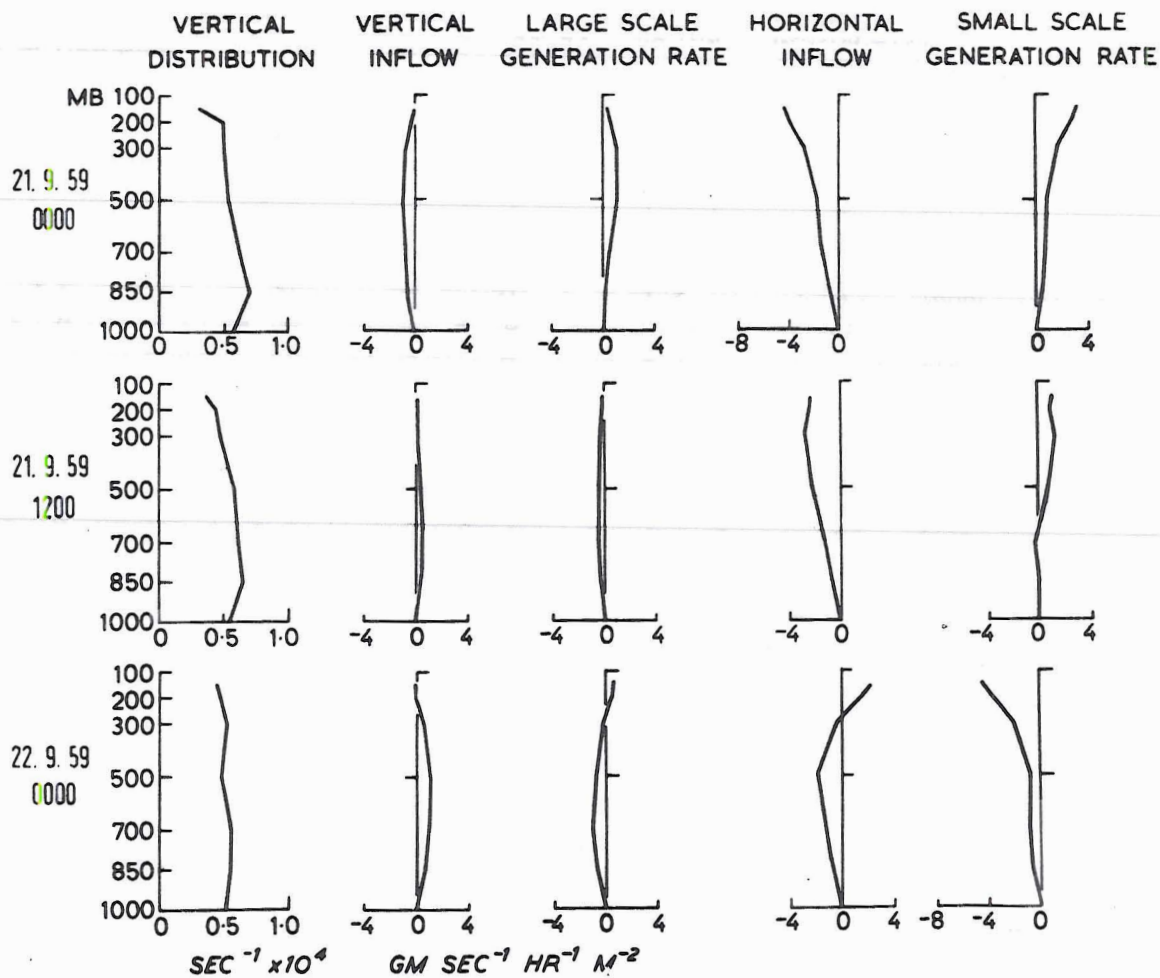


Fig. 11. Vorticity analysis. Case 4. 21-22 Sept. 1959. Wave moving westward at  $9 \text{ ms}^{-1}$  developing into hurricane to NE of area analysed.

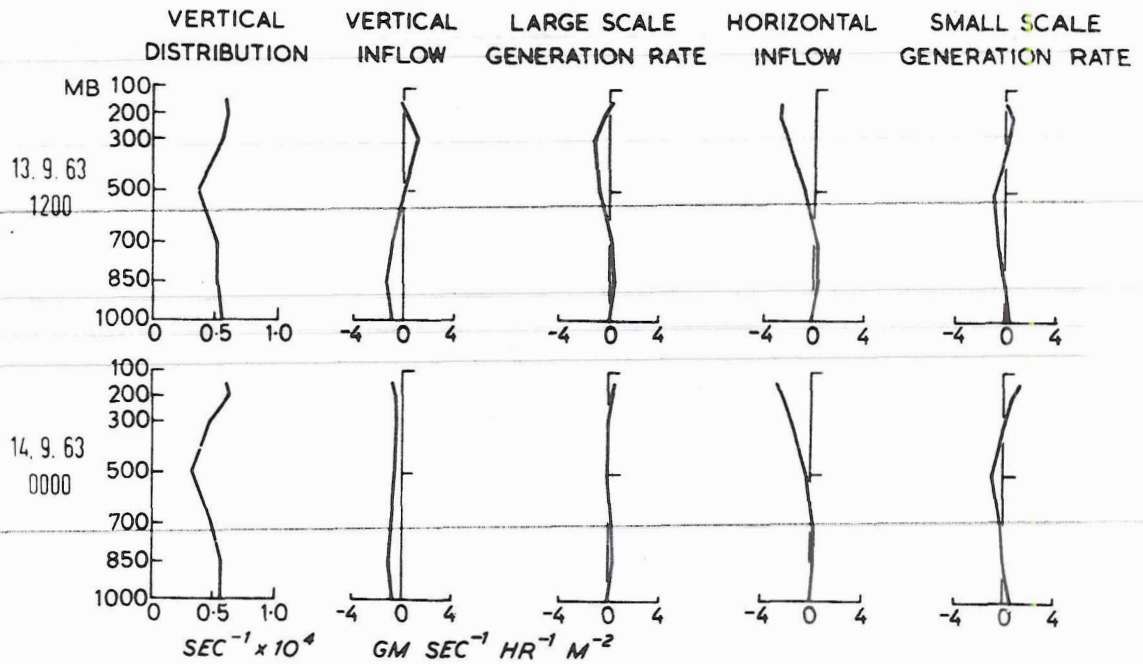


Fig. 12. Vorticity analysis. Case 5. 13-14 Sept. 1963.  
Non-developing warm core wave moving steadily  
westward at  $8 \text{ ms}^{-1}$ .

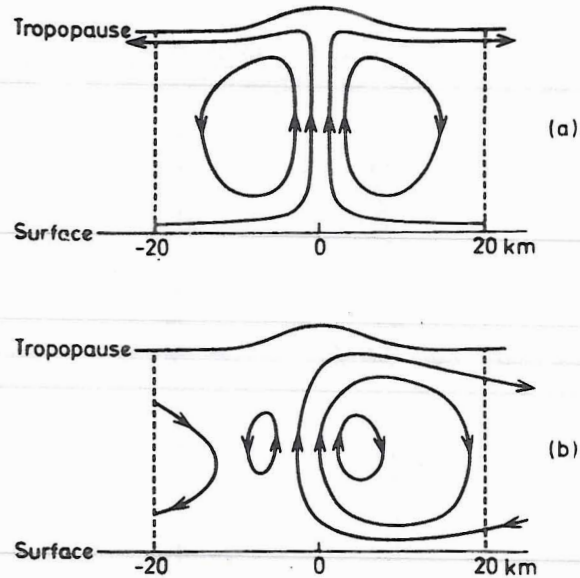


Fig. 13. Schematic streamlines of flow in fully developed cumulonimbus (a) without vertical shear, (b) with vertical shear. In both cases net mass inflow is assumed at lower levels and outflow at upper levels.

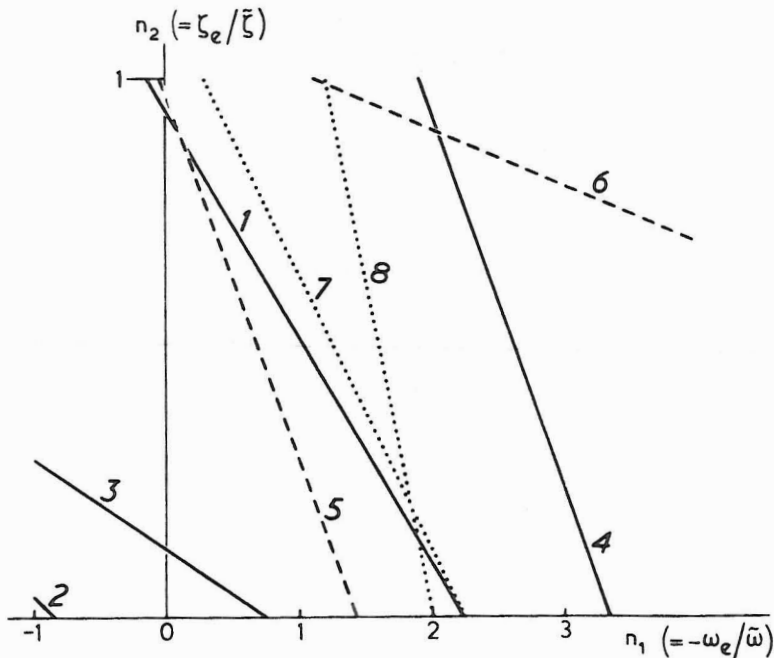


Fig. 14.  $\frac{z_e}{\bar{z}}$  computed as a function of  $-\frac{\omega_e}{\bar{\omega}}$  from Eq.(14), averaged for the central grid of 9 points and through the depth of the troposphere. Curves 1-4 refer to Case 3 (1200 3.10.58, 0000 and 1200 4.10.58 and 1200 5.10.58), 5 and 6 to Case 1 (0000 7.8.64 and 0000 8.8.64) and 7 and 8 to Case 2 (0000 and 1200 15.9.58).